Autoantibodies in maternal serum predict spontaneous preterm delivery

Elze Rackaityte[1], Beltran Borges[2,3,4], Shirley J. Shao[5], Joseph S. Creery[6], Hannah M. Kortbawi[1], Haleigh S. Miller[1], Margareta Mayer[4,7], Elaine Kouame[4,7], Sabrina A. Mann[1,6], Frank McCarthy[6], Scott Oltman[8,9], Kelsey C. Zorn[1], Andrew F. Kung[1], Anthea Mitchell[1,6], Gabrielle Rizzuto[11], Rebecca J. Baer[8,9,10], Caleigh Mandel-Brehm[1], Kelli K. Ryckman[12], Stephanie L. Gaw[5], Sara L. Hillman[13], Laura L. Jelliffe-Pawlowski [8,9], Joanna Halkias[4,7], Nasim C. Sobhani[5], Joshua E. Elias[6], Tippi C. MacKenzie[2,3,4], and Joseph L. DeRisi[1,6,*]

AFFILIATIONS

[1] Department of Biochemistry and Biophysics, University of California San Francisco, San Francisco, CA USA
[2] Department of Surgery, University of California San Francisco, San Francisco, CA USA
[3]Center for Maternal-Fetal Precision Medicine, University of California San Francisco, San Francisco, CA USA
[4]The Eli and Edythe Broad Center of Regeneration Medicine and Stem Cell Research
[5]Department of Obstetrics and Gynecology and Reproductive Sciences, University of California, San Francisco, CA USA
[6]Chan Zuckerberg Biohub San Francisco, San Francisco, CA, USA
[7]Division of Neonatology, Department of Pediatrics, University of California San Francisco, San Francisco, CA USA
[8]Department of Epidemiology & Biostatistics, University of California San Francisco, San Francisco, CA USA
[9]UCSF California Preterm Birth Initiative, San Francisco, CA, USA
[10]Department of Pediatrics, University of California San Diego, La Jolla, CA USA
[11]Human Oncology & Pathogenesis Program and Department of Pathology & Laboratory Medicine, Memorial Sloan Kettering Cancer Center, NY, NY USA
[12]Department of Epidemiology and Biostatistics, School of Public Health-Bloomington, Indiana University, Bloomington, IN USA
[13]Maternal and Fetal Medicine Department, Institute for Women's Health, University College London, London, United Kingdom.

*Correspondence should be addressed to Joseph L. DeRisi joe@derisilab.ucsf.edu

SUMMARY

Complications from preterm birth are the leading cause of global mortality in children under age five[1,2]. Spontaneous preterm labor is the most common cause of preterm delivery and is associated with a breakdown of maternal-fetal tolerance[3–5]. However, the current understanding of the role of autoantibodies in this process has been limited to a handful of examples of pathogenic antibodies that occur with pregnancy complications[6–14]. Here, we employ proteome-wide autoantibody profiling via phage display immunoprecipitation and sequencing (PhIP-seq) to identify autoreactivities associated with imminent preterm delivery in maternal sera across four cohorts of human pregnancy (n=1,023). We find that spontaneous preterm pregnancies exhibit greater proteome-wide autoreactivity, validated by placental proteome immunoprecipitation mass spectrometry analysis using patient sera. Within the preterm birth associated autoreactive signature, we find enrichment for pathways known to be critical for normal pregnancy outcomes, including vascular development, reproductive hormones, and regulators of inflammation. Further analysis of autoreactive targets revealed involvement of the IL1β inflammatory cytokine cascade. IL1β is one of the few inflammatory cytokines sufficient to rapidly induce labor in animals[15–24] and it is also elevated in preterm human pregnancies[25–29]. Across these four cohorts, antibodies to cytokine IL1 receptor antagonist (IL1RA), a natural antagonist to IL1β are significantly enriched in roughly 10% of preterm pregnancies and yet are completely absent in term pregnancies. Sera from these patients functionally neutralizes IL1RA activity *in vitro* and anti-IL1RA induces greater resorption, inflammation, and vascular malperfusion in timed-pregnant mice *in vivo*. These findings suggest utility for serologic diagnostics as one approach to stratify risk of spontaneous preterm delivery in addition to interventional strategies for management of IL1β during pregnancy.

MAIN TEXT

Globally, 10% of pregnancies result in preterm delivery which corresponds to an annual 15 million preterm births[2]. Preterm newborns, born before 37 weeks, are disproportionately vulnerable to sepsis, neuroinflammation, and respiratory distress[2]. Despite the high mortality associated with these complications and the costly burden to healthcare systems, there are currently no FDA-approved medications to prevent preterm delivery available in the US market[30,31]. While several maternal, fetal, and environmental factors have been associated with preterm birth, the lack of mechanistic understanding of disease pathophysiology hinders the development of effective diagnostics and therapeutics.

Preterm birth is a common symptom of multiple discrete pathologies. While 30-35% of preterm births are medically induced for maternal or fetal indications[1], the majority of preterm births (55-75%) occur spontaneously in the setting of preterm labor. Spontaneous preterm birth is often accompanied by preterm premature rupture of membranes (PPROM). These are also associated with infection and/or inflammation in approximately 30-40% of cases[1].

Although little is known about the causes of preterm labor in this clinical subset, animal studies have demonstrated that certain inflammatory cytokines are sufficient to induce labor[20]. Intrauterine injection of inflammatory cytokines, particularly IL1β, rapidly induces labor in non-human primates[20–24] and rodents[15–19]. This mirrors associations in humans, where elevated inflammatory cytokines are detected in mothers during labor, including spontaneous preterm labor[3,25–29].

The failure to establish or maintain maternal-fetal immune tolerance is also associated with spontaneous preterm birth[32]. Recently, tolerization of maternal B cells through antigen masking on the placenta has been implicated in the establishment of maternal-fetal tolerance[33]. However, our current understanding of the humoral immune system in this process in humans has been limited to a handful of examples of pathogenic autoantibodies that occur with pregnancy complications, such as

anti-RhD[6], anti-thyroid[12], anti-human platelet antigen[34], and anti-AT1 receptor[13,14] antibodies. Here, we describe the use of proteome-wide autoantibody profiling technologies to generate a comprehensive portrait of autoimmune reactivities in maternal sera that specifically precede spontaneous preterm birth.

Global remodeling of antibody specificity during pregnancy

To investigate autoreactivity during pregnancy, maternal sera from term and preterm pregnancies were used to determine antibody specificity in two cross-sectional pregnancy cohorts in addition to non-pregnant controls. Serum from these three cohorts was used to immunoprecipitate a customized, previously validated programmable phage display library of the human proteome with the PhIP-seq approach[35,36]. The first population-wide cohort of maternal sera was assembled from randomly selected maternal sera collected at collected at mean 16.5 weeks of gestation from a California-wide biobanking effort, with comparable numbers of preterm and term pregnancy outcomes and reflective of state demographics (**Supplementary Table 1**; **Fig 1a**; **Extended Data Fig 1a**; Cohort I; n=870; n=437 term, n=433 preterm). A secondary cohort was collected at a mean of 26.1 weeks of gestation from women experiencing spontaneous preterm labor complicated by PPROM or control pregnancies that delivered at term (**Supplementary Table 1**; **Fig 1a; Extended Data Fig 1b**; Cohort II; n= 64; n=38 term, n=26 preterm). Samples from healthy non-pregnant individuals (**Supplementary Table 1;** Baseline Cohort; n=101; n=49 male, n=51 female) served as additional controls. In total, 1,035 samples were analyzed for this initial phase. Following three rounds of phage enrichment, the encoded peptide inserts were sequenced and aligned to the input library to calculate overall enrichment as previously described[35]. A commercial anti-GFAP polyclonal antibody was used as a positive control (n=12). Peptides corresponding to the GFAP protein were enriched by an average of 3,601-fold relative to IPs with sera from the human cohort samples (**Extended Data Fig 2a**). Prior to any filtering, PhIP-seq immunoprofiles from healthy controls were investigated for batch effects. Peptide-level RPK PhIP-seq profiles did not differ across experimental batches by UMAP analysis (**Extended Data Fig 2b**) and a subset of samples that were technically replicated across experimental batches (n=27) exhibited high Pearson co-correlation (mean r=0.71) (**Extended Data Fig 2c**). A total of 293 consistently enriched peptides were identified in mock IPs and removed from downstream analysis (see Methods).

Peptide-level fold change relative to mock IP controls was calculated and a co-correlation analysis was performed to detect global differences amongst non-pregnant controls, preterm, and term pregnancies in Cohorts I and II (**Fig 1b).** Using a Pearson correlation threshold of 0.3 (**Extended Data Fig 3a**), the number of co-correlating patient pairs for each group of subjects was determined and expressed as “percent connectivity” (the number of connected subjects as a percentage of the total). Among non-pregnant controls, the percent connectivity was 22.9% (22 of 96), consistent with previous observations that PhIPseq signatures are highly individualized[37]. Percent connectivity among term uncomplicated pregnancies (n=208; see Methods) was 20.2%; however, the distribution of pairwise correlation coefficients was significantly greater than in non-pregnant controls (p adj=5.4e-44; **Extended Data Fig 3b**). While connectivity is relatively similar between non-pregnant and pregnant subjects, a greater degree of co-correlation suggests additional sharing of autoreactivity due to pregnancy itself. Term pregnancies with complications exhibited a slight increase percent connectivity (26.2%, n=229, p adj = 3.4e-30); however, the largest increase was observed in preterm pregnancies (40.0%, n=432; **Fig 1b**), with significantly greater correlation values (p adj= 3e-143; **Extended Data Fig 3b**). These results suggest complications and preterm pregnancies are accompanied by a pattern of autoreactivity this is, in part, shared, unlike term pregnancies or non-pregnant individuals.

Given that B cell memory to fetal antigens likely persists beyond gestation[9,38], the influence of gravidity (total number of pregnancies) on maternal autoantibody profiles was investigated. Percent

connectivity was greater in preterm multi- versus primigravida (33.4% vs. 21.1%; **Extended Data Fig 3c-d**) but not in term multi- versus primigravida (16.7% vs 12.5%; **Extended Data Fig 3c-d**). Greater connectivity was also noted in spontaneous rather than iatrogenic preterm pregnancies (**Extended Data Fig 3e**). These results suggest that repeated pregnancies are accompanied by increased sharing in autoreactive profiles in spontaneous preterm pregnancies.

The preterm autoantibody signature

The presence of increased autoreactive antibody sharing among preterm pregnancies as early as 16.5 weeks of gestation and preceding preterm delivery suggests that these data may be used to build classification models. First, feature selection was performed utilizing PhIP-seq data from Cohorts I & II. PhIP-seq autoreactive profiles were z-scored using the mean of enrichment values for uncomplicated term pregnancies. Peptides with a z-score of 3 or greater were designated as preterm specific if they were shared by at least two preterm subjects and were never significantly enriched in healthy term samples (z-score ≤ 3; **Extended Data Fig 4a**; **Supplementary Table 2**; see Methods). Conversely, term specific peptides were identified using the mean of the preterm samples to calculate z-scores. Preterm autoreactivities were significantly more shared across Cohort I and Cohort II than in term pregnancies (6,926 and 2,642 overlapping proteins in preterm and term, respectively; **Extended Data Fig 4b**), mirroring findings in Pearson co-correlation analysis (**Fig 1b**). Analysis of top peptides by prevalence, discussed in more detail below, revealed a highly specific, though sparse signal that preceded preterm delivery by an average of 15 weeks (**Extended Data Fig 5a; Supplementary Table 2)**.

Although PhIPseq provides proteome wide coverage, the substrates are restricted to largely linear peptides. To supplement this approach, immunoprecipitation mass spectrometry (IP-MS) may be used as a complementary technique to identify whole protein targets, including conformational epitopes present on full length proteins. A randomly selected subset of sera from Cohort II (n=13 term, n=25 preterm) was used to immunoprecipitate native proteins from placental extract. Antibody targets were identified using trapped ion mobility time of flight mass spectrometry (timsTOF-MS; see Methods). Unsupervised machine learning analysis of the enriched protein abundances yielded two clear clusters, distinctly segregating preterm or term samples (**Fig 1c**). Using the same mass spectrometry-derived protein abundances, a three-fold stratified cross-validated ridge-regularized logistic regression model was constructed (see Methods). Testing on a third of the data, held back from training, yielded models with a mean AUC of 0.88 ± 0.11 (**Extended Data Fig 4b**). Top ranked proteins by logistic regression coefficient revealed sharing across multiple individuals, and hierarchical clustering of these features clearly separated preterm versus term sera (**Fig 1d**; **Supplementary Table 3**). These data and strong classifier performance for both Cohort I and II support the notion that a multitude of early pregnancy serological indicators are predictive of spontaneous preterm delivery.

A conservative analysis pipeline was implemented by combining both PhIP-seq and IP-MS datasets from training Cohorts I & II to identify validated features that discriminate between term and preterm pregnancies (**Fig 2a**). The PhIP-seq-derived preterm signature from Cohort I was compared to enrichments from placental IP-MS data using Cohort II. Mass spectrometry-derived protein abundances were z-scored using the mean enrichment values for uncomplicated term pregnancies. Proteins with a z-score greater than 5 were considered to be preterm-specific if they were detected in at least one preterm subject and were never significantly enriched in healthy term samples. A total of 343 preterm proteins were identified by IP-MS (**Fig 2a**; **Extended Data Fig 6a**; see Methods). Among these, 65% (n=224 proteins) were also found by PhIP-seq and this defined the validated preterm autoantibody signature (**Fig 1d**; **Fig 2a; Extended Data Fig 6b**; **Supplementary Table 4**).

Prediction of imminent preterm delivery in validation cohorts

The number of preterm-specific autoreactivities were counted per sample and were found to be significantly higher in preterm versus term pregnancies in Cohorts I and II. Interestingly, the number of reactivities per subject increased with advancing gestation at sample collection (**Fig 2b**). To assess the consistency of preterm signature, two validation cohorts were examined. Cohort III was comprised of n=15 mother-infant dyads from term pregnancies, while Cohort IV was comprised of n=67 dyads from preterm pregnancies (**Fig 1a**). Using the preterm autoantibody signature (n=224 proteins), the cumulative enrichment of autoreactivities was measured (see Methods). Similar to Cohort I & II, there was a significantly greater sum of autoreactivity in preterm pregnancy measured from maternal serum, and this was also reflected in the infant compartment (cord blood; **Fig 2c**). Maternal connectivity was also significantly greater in preterm than in term pregnancies (76% vs 13%, **Extended Data Fig 6c**).

An ensemble model using the validated features of the preterm signature (n=224 proteins) was built to forecast preterm or term delivery from PhIP-seq data as input (see Methods). 1000 random five-fold splits of the data were run to obtain the envelope of model performance in Cohorts I and II. High accuracy and precision were detected across all models (mean ROC AUC of 0.98; **Fig 2d**), as expected for a training cohort from which the features were derived. The trained models with the best and worst performance were selected and used to predict preterm or term delivery in the validation cohorts (Cohorts III and IV), which were never used for training or feature selection. As expected, model performance on the validation cohorts was less than the training cohorts, however, strong forecasting ability was still achieved in both maternal and infant samples (ROC AUC 0.88 and 0.83, respectively; **Fig 2e**), indicating that the predictive model is generalizable and robust to overfitting. In both the training and validation cohorts, gestational age at sample collection was limited to the second trimester, which was matched across term and preterm pregnancies. To investigate the contribution of gestational age at sample collection on model performance, collection timepoints later in gestation from term pregnancies in Cohort III were analyzed. Compared to gestational age-matched samples to preterm in the second trimester, the forecasting ability deteriorated when the classifier was provided with third trimester and delivery timepoints from term pregnancies (ROC AUC 0.78 and 0.56, respectively; **Extended Data Fig 6d**). These data indicated that the preterm signature is highly specific to the second trimester, which would be an ideal timepoint for a population screening test. Prioritizing high sensitivity desired in screening tests, we selected a 0.8 true positive rate cut-off in the best performing model. A confusion matrix detected 2 false positives and 10 false negatives with a positive predictive value of 97% in maternal sera in validation cohorts III and IV (**Extended Data Fig 6e**). These results suggest that a sensitive and specific early screening test to predict preterm delivery could be developed from this non-invasive serological measure.

Targets within the preterm autoantibody signature

Population screening for preterm risk would likely be most useful when coupled with a targeted therapeutic. Autoantibodies can directly influence the function of their target proteins, therefore, we focused on grouping autoreactivities by predicted function of their targets. Patterns of autoantibody targets within the broader PhIP-seq preterm signature (**Extended Data Fig 5a**; **Supplementary Table 2**) were investigated using pathway gene-set enrichment analysis (see Methods). Significantly enriched pathways (adjusted p-value <0.05; 26 pathways) were manually grouped by their shared features. These included hormone synthesis and signaling, vascular cell development and function, muscle contractility, cell proliferation, and infection response categories (**Fig 3a, Extended Data Fig 7a-b**; **Supplementary Table 5**).

The placenta is a source of hormone production essential for the successful maintenance of pregnancy[39]. Interference or dysregulation of these pathways may lead to pregnancy complications or spontaneous preterm labor. Several critical reproductive hormones (and/or their receptors) were

significantly enriched. These included progesterone and estrogen receptors (PGR, ESR1, ESR2), prolactin (PRL, PRLR), human placental lactogen (CSH2), gonadotropins (CGA, GNRH2, GNRHR), follicular stimulating hormone receptor (FSHR), and relaxin receptors (RFXP1, RFXP3; **Fig 3a**; **Extended Data Fig 7c**; **Supplementary Table 5**). These data raise the possibility that preterm autoantibody specificities targeting reproductive hormones may contribute to a broader hormonal dysfunction observed in preterm pregnancies[40].

Vascular remodeling of maternal spiral arterioles is a hallmark of successful placentation. Proteases (e.g. ADAMTS13, VWF, F9) and canonical endothelial proteins (e.g. VE-cadherin, NOTCH, WNT) were significantly targeted in preterm pregnancies (**Fig 3a**; **Extended Data Fig 7c**). These targets pointed to potential defects in angiogenesis, vascular remodeling, and arterial differentiation, which are critical to the establishment of appropriate placental perfusion to the fetus. To validate these findings, we performed indirect immunofluorescence in placenta with ADAMTS13, a metalloprotease that cleaves von Willebrand factor. Autoantibodies to ADAMTS13 are associated with recurrent pregnancy loss and thrombotic thrombocytopenic purpura[41]. Interestingly, we find that ADAMTS13 was highly expressed on placental cytotrophoblasts (**Extended Data Fig 7d**), a finding that has been noted previously[42]. Another key remodeling protein enriched by preterm sera was VE-Cadherin, a protein essential for trophoblast invasion and spiral artery remodeling during placentation[43]. Indirect immunofluorescence localized VE-Cadherin to the endothelial cell-cell junctions (**Fig 3c**) in placental tissue consistent with previous reports[44]. The essential roles of these proteins, their expression on placenta, and their enrichment by preterm sera suggests the possibility that some of the corresponding autoantibodies may possess pathologic function-blocking activities related to pathways that maintain successful pregnancy.

Sterile and infectious inflammation are the most frequently identified causes of spontaneous preterm labor[1]. Preterm autoantibody targets in the infection response category included histocompatibility proteins (HMHA1, HLA-A, HLA-B, HLA-C, HLA-DMA, HLA-DOA, HLA-DOB, HLA-F, HLA-E) and the placental-specific HLA-G (**Fig 3a**; **Extended Data Fig 7c**; **Supplementary Table 5**). Anti-HLA antibodies increase the risk of spontaneous preterm delivery[45] and are associated with complement deposition in the placental endothelium, which occurs more frequently in spontaneous preterm labor[7]. Anti-cytokine antibodies, known to increase susceptibility to infection[46], were also identified. Of these, anti-IL1RA and anti-IL16 were the most significantly enriched. Anti-IL1RA was the only anti-cytokine reactivity that was present in all three preterm pregnancy cohorts both by PhIP-seq and IP-MS (**Fig 3a**; **Fig 1d**).

Neutralizing anti-IL1RA autoantibodies define a subset of spontaneous preterm pregnancies

Given the established role of IL1β for the promotion of labor[20], identifying the secreted competitive antagonist, IL1RA, as a consistently enriched autoreactive target was intriguing. Therefore, we focused on antibodies to IL1RA, encoded by the IL1RN gene. The prevalence of anti-IL1RA positive preterm pregnancies was 9.5% in Cohort I by PhIPseq, and 20% of preterm sera by IP-MS in Cohort II (**Fig 3b**). Sera remaining from three out of four anti-IL1RA positive Cohort II samples were tested in a native ELISA with supernatants from IL1RA over-expression in HEK293T cells. Sera from these preterm pregnancies resulted in significantly greater ELISA signal compared to known anti-IL1RA negative term pregnancies (**Fig 3b**). To investigate localization of IL1RA in human tissues, we used a commercial antibody to IL1RA (Sigma Prestige HPA001482) to detect localization of IL1RA in placenta by indirect immunofluorescence analysis. A striking pattern of IL1RA localization was found near CD31-positive fetal vessels within the placenta (**Extended Data Fig 8a-c**) that also co-localized with VE-cadherin in endothelial cell junctions (**Fig 3c**). While IL1RA is known to be secreted, these results suggest a substantial amount of this protein is localized to the endothelial adherens junctions in the placenta.

To address whether the observed pattern of IL1RA co-localization was authentic, or due to cross reactivity of the antibody with other targets, PhIP-seq was performed with the same antibody and analyzed for enrichment. Only the IL1RA derived peptides were enriched above background, suggesting the commercial IL1RA antibody is highly specific (**Extended Data Fig 8d**). As a further validation of antibody specificity, a blocking assay was performed with the peptide immunogen used to generate the antibody (**Extended Data Fig 8e**). The signal corresponding to IL1RA was eliminated, again suggesting this antibody is highly specific (**Extended Data Fig 8f**). Together, these data support the notion that IL1RA is bound at placental endothelial cell junctions, in close proximity to other junction proteins, like VE-cadherin. To our knowledge, this is the first report demonstrating localization of IL1RA to endothelial junctions of the placenta.

To further validate the presence of anti-IL1RA antibodies in patient sera, we investigated whether anti-IL1RA$^+$ patient sera was capable of blocking IL1RA on placental tissue from binding by a commercial antibody. A positive result would further confirm the existence and specificity of anti-IL1RA antibodies with respect to native placental tissue bound IL1RA protein. Flash frozen placenta was first blocked with either PBS or term or anti-IL1RA$^+$ patient sera, and then indirect immunofluorescence was performed with the commercial anti-IL1RA antibody (see Methods; **Extended Data Fig 8g**). The characteristic pattern of IL1RA localization to fetal vessel cell-cell junctions was clearly observed in in the absence of sera, term sera or anti-IL1RA$^-$ preterm sera (**Fig 3d**; **Extended Data Fig 8g**). However, IL1RA localization signal was blocked in placental tissue treated with anti-IL1RA$^+$ preterm sera (**Fig 3d**; **Extended Data Fig 8g**). These data strongly support the presence of highly specific anti-IL1RA$^+$ autoantibodies in the maternal sera of a subset of preterm pregnancies, and that these antibodies readily bind native tissue bound IL1RA in normal placenta.

To identify the epitope on IL1RA targeted by anti-IL1RA$^+$ pregnancies, peptide fragments from PhIP-seq and IP-MS were analyzed. Positional mean enrichment analysis of PhIP-seq data (see Methods) revealed that the majority of anti-IL1RA$^+$ pregnancies targeted overlapping peptides between D99-D129 amino acid residues on IL1RA. This epitope (**Fig 4a**; **Extended Data Fig 9a**), opposite the receptor engaging face, is highly charged and contains the only N-linked glycosylation residue in the protein (N109)[47,48]. Antibodies to this epitope have previously been reported in IgG4 disease[49] and we discovered that it is also targeted by two commercial antibodies (**Fig 4a**; **Extended Data 9a**). IP-MS fragment analysis identified a single 16 amino acid peptide (103-LQLEAVNITDLSENRK-118) that was fully contained within the target PhIP-seq fragment (**Fig 4a**; **Extended Data 9a**). These data confirm the target epitope enriched by both PhIP-seq and IP-MS are localized to the same region, and furthermore, these data suggest that anti-IL1RA antibodies present in multiple pre-term sera converge on the same region of the protein.

To investigate the functional consequences of anti-IL1RA antibodies, a previously described IL1β reporter cell line and validated assay was utilized[49–51]. Briefly, neutralization of IL1RA was measured using a reporter cell line in which IL1 receptor activity results in secreted embryonic alkaline phosphatase (SEAP). Reporter cells were stimulated with recombinant IL1β and a titration of increasing amounts of excess of IL1RA and serum or antibody (**Extended Data Fig 9b-d**), SEAP rates were normalized to the negative control (TNFα treated cells) and an IL1β activity index was calculated for cells stimulated with IL1RA and IL1β relative to IL1β alone (see Methods). Compared to cells treated with PBS or off-target anti-GFAP antibody, a commercial anti-IL1RA antibody (R&D AF-280-NA) that primarily targets the patient epitope (**Extended Data Fig 9a**), resulted in significant neutralization of IL1RA as measured by greater IL1β activity (**Fig 4b**; **Extended Data Fig 9c**). Similarly, anti-IL1RA$^+$ preterm sera also resulted in significantly higher IL1β activity (**Fig 4c**; **Extended Data Fig 9d**). Conversely, cells treated with PBS, male, or term sera exhibited low IL1β activity. Thus, both commercial antibodies and preterm patient sera are sufficient to neutralize IL1RA antagonist, thus permitting increased IL1β signaling.

Maternal anti-IL1RA antibodies promote fetal resorption and malperfusion in vivo

To further explore the physiological consequence of circulating anti-IL1RA antibodies *in vivo,* the role of maternal anti-IL1RA antibodies was investigated during murine pregnancy. We hypothesized that since IL1RA regulates IL1β, adoptive transfer of anti-IL1RA antibodies would inhibit the ability of IL1RA to rescue pregnancies threatened by IL1β-induced inflammation, resulting in worse pregnancy outcomes (**Extended Data Fig 9e**). First, we confirmed that the patient epitope targeting commercial anti-IL1RA antibody was cross-reactive to the native mouse orthologue by dot blot (**Extended Data Fig 9f**). Timed-pregnant dams were injected intravenously three times (Embryonic Days 13.5-15.5; E13.5-15.5) with either the anti-IL1RA antibody or an equivalent amount of isotype control in the context of IL1β-induced inflammation (**Fig 4d**). Levels of murine il1β were measured in maternal serum by ELISA on the day before expected delivery (E18.5). Concentration of Il1β was significantly greater in anti-IL1RA injected dams as compared to isotype controls (**Fig 4e**), indicating that anti-IL1RA neutralizes the ability of the antagonist to regulate Il1β during pregnancy. Anti-IL1RA injected dams also exhibited profound reproductive defects. Resorption rate was significantly elevated (**Fig 4f**). Among the non-resorbed pups, a significantly greater proportion of fetuses from anti-IL1RA pregnancies exhibited less prominent cephalic vasculature and pallid skin color (**Fig 4g-h**; **Extended Data Fig 9g**), suggestive of a defect in perfusion. Malperfused pups weighed significantly less than normal pups, though a defect in gross placental weight was not observed (**Extended Data 9h-j**). Cephalic vasculature was quantified from images of pups (see Methods) and was significantly lower in anti-IL1RA treated pregnancies than isotype controls (**Extended Data Fig 9k**). Together these data indicate that anti-IL1RA antibodies are capable of functionally inhibiting IL1RA antagonism of the IL1β pathway and lead to resorption as well as vascular defects in placenta and fetus *in vivo*.

DISCUSSION

Prior work has demonstrated that certain pathogenic alloantibodies are capable of driving pregnancy complications in humans[6,12,13]. By investigating human proteome-wide reactivity in over 1,000 maternal sera, our data provide a comprehensive portrait of autoreactivity in preterm pregnancies relative to term. Currently, identifying early risk for preterm birth is limited to negatively predicting preterm delivery within seven days of delivery[52], which is not recommended for clinical use by the American College of Obstetrics and Gynecology[53]. We identified a preterm-specific autoreactive signature that preceded spontaneous preterm delivery by an average of 15 weeks. A compact set of features was selected for the forecasting model and experimentally validated with two orthogonal approaches (PhIP-seq and IP-MS). Our classifier forecasted preterm delivery in two independent validation cohorts, comprised of pregnancies from the US and the UK with varied racial and ethnic representation. These data suggest that maternal immunity may be predisposed to spontaneous preterm labor as early as the second trimester and that a serum antibody assessment may yield clinical utility for a universal early screening of risk. Developing such a non-invasive diagnostic could inform pregnant mothers to receive care at hospitals with expertise in preterm neonatal care, allowing for effective delivery of life-saving neonatal interventions[54]

Prediction of imminent preterm delivery will be most useful if an effective and early intervention or therapeutic is also available. Currently there are no treatments in clinical practice to prevent spontaneous preterm birth, although delivery of preterm infants in centers with dedicated neonatal intensive care does improve outcomes. In this work, a subset of preterm pregnancies was defined by the presence of anti-IL1RA antibodies in maternal serum. This subset, which would extrapolate to roughly 2 million global preterm births per year, exhibited deficiencies in regulating the labor-promoting IL1β pathway *in vitro* and *in vivo*. Recombinant IL1RA is an FDA-approved drug (anakinra, also known as Kineret, SOBI, Inc) for treatment of rheumatoid arthritis and neonatal onset

405 multisystem inflammatory disease (NOMID; also known as chronic infantile neurologic, cutaneous,
406 articular syndrome)[55]. The finding of anti-IL1RA antibodies in preterm birth sera suggests that
407 administration of exogenously supplied IL1RA may have the effect of mitigating the negative
408 consequences of unchecked IL1β signaling. In this subset of women, the presence of anti-IL1RA
409 antibodies suggests that the use of anakinra may be of therapeutic value for the prevention of
410 preterm delivery. These results also suggest derivatives of IL1RA, lacking the epitope binding
411 sequences, may evade autoantibodies in some patients.
412
413 The cross-sectional studies presented here do not address when or why IL1RA antibodies emerge
414 with respect to the chronology of pregnancy, or whether these antibodies are already present, even
415 before pregnancy. Indeed, antibodies to IL1RA have been previously reported in the context of
416 COVID infection[51], IgG4 disease[49], and Still's disease[56] and thus their presence may be independent
417 of pregnancy. However, we demonstrate that the placenta also expresses high levels of IL1RA which
418 may lead to sensitization to IL1RA during a breakdown of maternal-fetal tolerance. Certain IL1RA
419 alleles are associated with PPROM[57], supporting the idea that an allelic mismatch between mother
420 and fetus may lead to immune sensitization. Longitudinal studies will be required to determine the
421 timing of anti-IL1RA antibody generation with respect to pregnancy, the mechanisms of anti-IL1RA
422 origins, and the critical window for a serum test.
423
424 Together, these results lay the foundation for the development of rapid, non-invasive, and cost-
425 effective serological diagnostics for the early prediction of spontaneous preterm delivery. This
426 diagnostic approach, combined with a targeted therapeutic intervention to limit the effects of
427 autoantibody targets, promises improved management of pregnancies at risk for preterm delivery and
428 reductions in neonatal morbidity and mortality.
429
430
431 **METHODS**
432
433 *Human cohorts and samples*
434 Sera from the Cohort I was obtained from a California-wide biobank. Sera from the Cohort II and
435 Cohort III was obtained from deliveries at UCSF under IRB approved protocols. Sera from Cohort IV
436 was obtained from UCL Hospital and Homerton University Hospital of the National Health Services of
437 the United Kingdom, under UCL and UCSF approved IRB protocols. An uncomplicated, term
438 pregnancy was defined as one resulting in delivery at greater than or equal to 37 weeks of gestation
439 and did not have a diagnosis of any of the following: placental abruption, placenta previa,
440 chorioamnionitis, oligohydraminos, polyhydraminos, premature rupture of membranes, bacterial
441 vaginosis, urinary tract infection, diabetes or gestational diabetes, preexisting or gestational
442 hypertension, preeclampsia, infection during pregnancy, any specified placental condition, retained
443 placenta with or without hemorrhage, unspecified hemorrhage, abnormal clotting, or threatened
444 abortion. Any pregnancy that required transfusion, rhesus isoimmunization, or cerclage was excluded
445 from this group. We also excluded mothers with any hypertension disorder, endometriosis, Group B
446 streptococcus positivity, any coagulation deficiency, malignancy, asthma, allergic dermatitis,
447 anaphylaxis, rheumatoid arthritis, systemic lupus erythematosus, autoimmune thyroiditis, or mental
448 disorder. Mothers who reported any smoking, drug or alcohol abuse or dependency during pregnancy
449 were excluded. Pregnancies where the infant exhibited convulsions, abnormal neural imaging or
450 exam, retinopathy of prematurity, respiratory distress syndrome, intraventricular hemorrhage,
451 necrotizing enterocolitis, bronchopulmonary dysplasia, periventricular leukomalacia, hypoxic-ischemic
452 encephalopathy, or known congenital heart disease were also excluded from this group. Finally, we
453 also required that women defined as having uncomplicated pregnancies did not have a history of
454 recurrent pregnancy loss, preterm delivery, or poor obstetric/reproductive outcomes.
455

Term pregnancies with one or more of the above were considered medically complicated. Preterm pregnancies were defined as those delivering prior to 37 weeks of gestation and were further subdivided into spontaneous (including preterm premature rupture of membranes) or iatrogenic preterm delivery.

Non-pregnant controls were obtained from the New York Blood Center, as previously described[58].

PhIP-seq with human peptidome library

The human T7 phage display library used for immunoprecipitation and sequencing is previously described and sera from the above cohorts was used in high-thruput protocols as previously described. Detailed protocols are published on protocols.io DOI: dx.doi.org/10.17504/protocols.io.4r3l229qxl1y/v1

Trapped Ion Mobility Time of Flight Mass Spectrometry of Immunoprecipitated Placental Protein Lysate

Term placenta from a single donor was harvested within 2 hours of delivery. Implantation side of placenta was dissected to 1 cm^3 blocks and flash frozen in liquid nitrogen. Placenta protein lysate was prepared by mechanically dissociating tissue using a glass Dounce homogenizer and an electric tissue homogenizer in RIPA buffer with protease inhibitors (Roche) on ice. Protein was quantified using Bradford Assay (Pierce), normalized to 500µg in TNP40 and incubated with 1µL of human sera overnight at 4C with overhead mixing. Proteins were subsequently incubated with a 1:1 mix of protein A and protein G Dynabeads (Thermo) for 1 hour and washed five times with RIPA and once with TrisHCl. A NanoDrop reading was taken under TrisHCl to quantify protein.

Supernatant was removed and proteins were then resuspended in 8M urea, 50mM Tris (pH 8) before being subject to a standard on-bead protein digestion. The protein digestion procedure included disulfide reduction with 5 mM DTT, alkylation with 14 mM iodoacetamide, and an overnight digestion with Lys/C at a protein to protease ratio of 1:50. In order to obtain an optimal tryptic digestion, the urea concentration was then diluted to 2 M with 50 mM Tris (pH 8) followed by the addition of trypsin to a protein to protease ratio of 1:50, and a 4 hour incubation at room temperature. The peptide supernatant pH was then decreased to 2 with 7 µL formic acid (FA) and separated from the beads with a magnet. An extraction was performed on the beads by resuspension with 0.1% FA, the supernatant of which was added to the final sample. Peptide desalting was performed with the AssayMAP Bravo (Agilent Technologies) using a standard RPS peptide cleanup cartridges and protocol[59]. Approximately 25 ng of desalted peptides were analyzed on a TIMSTOF SCP mass spectrometer (Bruker Corporation) coupled with an EASY-nLC 1200 LC system (Thermo Fisher Scientific). Peptides were separated by reverse-phase chromatography on a 25 cm column (75-µm inner diameter, packed with 1.6 µm C18 resin, AUR2-25075C18A-CSI; IonOpticks). Peptides were introduced into the mass spectrometer using a gradient starting with 2% to 8% buffer B (0.1% (v/v) formic acid in 80% acetonitrile) for 1 min followed by an increase to 25% buffer B for 25 min then an increase to 40% buffer B for 5 min at a flow rate of 100 nL/min and were ionized by CSI (captive spray ionization).

Samples were first analyzed by PASEF-dda with a duty cycle of 1.03 sec comprising one MS1 survey for every 5 PASEF MS2 ramps and a mass range between 100 and 1700 m/z. The TIMS device ramp/accumulation time was set to 166 ms with a 100% duty cycle and a mobility range of 0.7 to 1.3 1/K0. Precursor ions from the survey scan were selected using an adjusted isolation width of 2 m/z below 700 m/z and 3 m/z above 800 m/z precursor mass-to-charge value in the quadrupole that aligns with the anticipated TIMS elution time relative to the ion mobility value. Fragmentation was performed by Collision Induced Dissociation (CID) with CE (collisional energy) interpolation between 42 eV at 0.65 1/K0, 31.92 eV at 0.8 1/K0, 36.96 eV at 1 1/K0, 42 eV at 1.2 1/K0, 47.04 eV at 1.4 1/K0

508 and 51.24 eV at 1.6 1/K0. Active exclusion of precursors were released after 0.2 minutes. Precursor
509 repetitions were set to a target intensity of 20000 and a threshold of 500.
510
511 Real-time searching was performed with PaSER (Parallel Search Engine in Real-Time) against a
512 human Uniprot database (downloaded on 30 July 2022) using a reverse-decoy method with default
513 settings. A spectral library was generated from the searched DDA data using PaSER. Samples were
514 then analyzed by PASEF-dia using a high speed acquisition scheme from Meier F et al and
515 searched in real-time against the DDA generated spectral library using the TIMS DIA-NN algorithm
516 with default settings.
517
518 Peptide counts were collapsed to the corresponding protein, log-normalized, and fold changes and z-
519 scores were calculated over mean signal in term pregnancies. Preterm-specific hits were identified by
520 requiring that at least one preterm pregnancy and no term pregnancies met the threshold of z>=5 for
521 a given protein.
522
523 *ELISA with HEK293T IL1RA Overexpression Supernatant*
524 HEK293T cells (ATCC-CRL3216) were plated at 30% density in complete DMEM media (Sigma) with
525 Glutamine, 10%Fetal Bovine Serum (FBS), 50 ug/mL of Streptomycin and 50 I.U/ml of Penicillin.
526 cells were plated on standard 10cm^2 tissue culture dishes. Following plating, cells were allowed to
527 seed for 24 hours and subsequently transfected with experimental plasmids using a standard calcium
528 phosphate transfection method. One microgram of pCMV6 IL1RA overexpression plasmid (Origene
529 Cat. No. RC218518) was transfected per 10 cm^2 dish. Ninety-six hours following transfection
530 supernatant was harvested and normalized using a standard Bradford assay. Western blot analysis
531 confirmed IL1RA expression in supernatant (data not shown). A sandwich ELISA was performed
532 using standard protocols by capturing IL1RA from supernatant using goat anti-human IL1RA antibody
533 (R&D AF-280-NA) and detecting by utilizing a dilution of patient serum. Bound anti-IL1RA from
534 human serum was detected with an anti-human HRP and quantified with standard protocols.
535
536 *Placental Immunofluorescence*
537 Placental tissue was harvested within 2 hours of delivery and embedded, unfixed, in O.C.T compound
538 (Tissue-Tek) and flash frozen in an isopentanol bath submerged in liquid nitrogen. Ten-micron
539 cryosections were cut from frozen blocks and adhered to glass slides. Slides were thawed and briefly
540 post-fixed with acetone, rehydrated in 1x PBS, blocked with 10% (v/v) goat serum in 1x PBS for 2
541 hours, and incubated with 1:1000 rabbit anti-human anti-IL1RA (Millipore Sigma Cat No. HPA001482)
542 and 1:500 rat anti-human CD31 (Abcam Cat. No. ab9498) overnight at 4C in a humidified chamber.
543 Primary antibodies were washed using standard protocols and incubated with anti-rabbit and anti-rat
544 secondaries using standard protocols. Secondary only controls were stained identically but omitting
545 primary antibody. Stained tissue was imaged using the Crest LFOV Spinning Disk/ C2 Confocal at
546 400x magnification under identical camera exposure and laser settings for secondary only and
547 experimental samples. Micrograph exposure was normalized to secondary only negative control in
548 FIJI and applied to all images at once. In peptide blocking experiments, IL1RA PrEST Antigen
549 (Millipore Sigma APREST83081) was incubated with anti-IL1RA antibody per manufacturer's
550 instructions at 4C overnight and used to stain tissue as above. In serum blocking experiments,
551 placental sections were blocked with 1% (v/v) goat serum and 10% human serum in PBS-T overnight
552 at 4C. Controls were blocked without human serum. Placenta was subsequently probed with the
553 commercial anti-IL1RA antibody (Millipore Sigma Cat No. HPA001482) and imaged as above.
554
555 *In vitro IL1RA blocking assay*
556 Diluted patient sera, anti-IL1RA (R&D AF-280-NA), or anti-GFAP were pre-incubated with human IL1-
557 RA (Peprotech) overnight and applied to the HEK-Blue IL1β cells (InvivoGen) for 2 hours. Cells were
558 subsequently stimulated with human IL1β (Peprotech) for 72 hours at 37C. Cells treated with IL1β
559 alone or TNFa alone (Peprotech) were used as positive and negative controls, respectively.

Supernatants were assayed using the QANTI-Blue assay (InvivoGen), as previously described[49,51]. IL1β activity index was calculated by measuring SEAP activity at OD_{655} every 15 minutes for 2 hours and determining the rate of enzymatic activity. Slopes were background subtracted (cell treated with TNFa) and normalized to mean signal in IL1β treated cells. IL1β activity index was defined as the fold change of signal in serum or antibody treated cells over signal in cells incubated with IL1RA and IL1β only. Each experiment was carried out in triplicate for a total of three biological replicates.

Murine Il1ra dot blot

500 or 250 nanograms of recombinant mouse Il1ra (R&D 480-RM-050) were blotted onto nitrocellulose using a custom 3D printed dot blot device under vacuum. Membranes were blocked for 1 hour at room temperature in 5% (w/v) milk and subsequently probed overnight at 4C with either anti-human IL1RA antibodies (R&D AF-280-NA or Sigma Prestige HPA001482) or anti-mouse Il1ra antibodies (Invitrogen PA5-21776 or R&D MAB4801) or no primary antibody. Following standard washing procedures, membranes were probed with relevant secondaries conjugated to Licor-IR dyes and blots were imaged using the Licor Odyssey machine. Membranes were imaged together in one scan under identical exposure settings.

Animal Husbandry and Injections

All mice were housed, bred, and maintained in a pathogen-free facility at the University of California San Francisco (UCSF). All procedures were performed in concordance with UCSF Institutional Animal Care and Use Committee (IACUC) regulations and approved protocol. Timed-pregnant C57BL/6 females were purchased from Jackson Laboratories (strain #000664). Retro-orbital (RO) injections were done following with UCSF IACUC procedural guidelines. Briefly, pregnant dams were anesthetized at E13.5-E15.5 with isoflurane and injected in the RO sinus using 0.5mL insulin syringes, with a maximum volume of 150μL containing 5μg of human IL1β (Peprotech 200-01B) and 50μg of polyclonal goat IgG (isotype control; R&D AB-108-C) or of goat anti-human IL1RA antibody (R&D AF-280-NA) in sterile PBS. Reagents were mixed immediately prior to injection.

Mouse harvesting

Mice were euthanized at E18.5 with CO_2 and a sample of serum was obtained via transcardial puncture. Resorbed and malpefrused fetuses were quantified. Whole fetuses and their placentas were harvested and weighed. Murine Il1b concentrations were measured in maternal serum by a commercial ELISA (Abcam Cat No. ab197742). Cephalic vasculature was quantified from images of dissected fetuses using the Vessel Analysis plug-in for ImageJ[61].

Bioinformatic Analyses

To analyze peptide enrichment after PhIP-seq, reads were aligned at the protein level using RAPsearch[62], as previously described . Aligned reads were normalized to 100,000 reads per k-mer (RPK) to account for varying read-depth. All downstream analyses were performed by using an implementation of PhagePy python package (https://github.com/h-s-miller/phagepy). All data was initially filtered to exclude peptides found in mock IPs by calculating log-transformed fold changes over mean in mock IPs. These were z-scored and peptides with a z-score greater than 3 in a minimum of 3 experimental samples and no mock IP samples were carried to downstream analysis. Post-normalization batch effect was not observed.

Auto-correlation between technical replicated samples and individual samples was evaluated by Pearson correlation. Percent connectivity was calculated by dividing the number of nodes that retained a connection after filtering based on Pearson correlation cut-offs by the total number of nodes (samples) for a given group.

Preterm- or term-specific candidate autoreactivities were identified by calculating log-fold changes over mean term or preterm samples and z-scores were derived to identify enriched peptides within each individual relative to controls. Peptides with z-scores greater than or equal to 3 were considered hits and either preterm- or term-specific peptides were identified by filtering by requiring that the peptide was a hit in at least 2 cases and zero controls. Positional enrichment analysis across IL1RA was performed as previously described[64]. Unsupervised clustering was performed using UMAP implementation in the scikit-learn package in python. Autoreactivities were counted per person by summing up binarized per peptide hits within the preterm-specific PhIP-seq signature identified in Cohorts I and II. Cumulative enrichment in Cohorts III and IV was calculated by summing log-transformed enrichments over mock IPs for peptides identified as preterm specific by IP-MS and PhIP-seq in Cohorts I and II. GSEA analysis was performed utilizing the gseapy package utilizing the "KEGG_2021_Human" and "Panther_2016" databases.

Machine Learning Predictive Modelling

An initial classifier was derived from IP-MS data for Cohorts I and II implemented in scikit-learn in python. For the initial IP-MS model, feature selection was not performed. Log-transformed peptide abundances were input into fitting with a ridge-regularized logistic regression model with the saga solver across stratified three-fold cross validation. A ROC curve was utilized to analyze models across the cross-validation folds.

The final forecasting model utilized features identified in Cohorts I and II from both PhIP-seq and IP-MS data. Peptides identified as preterm specific in PhIP-seq data were filtered to their corresponding proteins that were also identified as preterm-specific in IP-MS datasets (see above). The overlapping 224 proteins defined the preterm-specific signature. Hit counts of preterm specific peptides in Cohort I and II belonging to these 224 proteins were summed and all peptides belonging to the 224 proteins were additionally summed. These features were used to train a new ensemble model implemented in scikit-learn pipeline in python using Cohorts I and II as the training set. The data was scaled using a standard scaler, and an ensemble voting classifier with soft voting between ridge-regularized logistic regression and a native bayes gaussian model. The best performing classifier from a stratified, shuffled five-fold cross validation was used to predict on Cohorts III and IV. We utilized completely independent cohorts for validation that were never included in the training phase, ensuring a lack of data leakage. Log-transformed PhIP-seq data normalized to mock IP (see above) from Cohorts III and IV was used as input and summed across features identified in Cohorts I and II as described above. ROC AUC curve analysis and a confusion matrix were used to evaluate model performance in this validation dataset.

Data Availability

All raw and processed data, the forecasting model and feature weights, as well as the associated code are available for download at Dryad (https://doi.org/ 10.5061/dryad.fqz612k24). PhIP-seq analytical code is freely available on GitHub: https://github.com/h-s-miller/phagepy

662
663 **REFERENCES**

664 1. Goldenberg, R. L., Culhane, J. F., Iams, J. D. & Romero, R. Epidemiology and causes of preterm
665 birth. *Lancet (London, England)* **371**, 75–84 (2008).
666 2. Liu, L. *et al.* Global, regional, and national causes of under-5 mortality in 2000–15: an updated
667 systematic analysis with implications for the Sustainable Development Goals. *The Lancet* **388**,
668 3027–3035 (2016).
669 3. Törnblom, S. A. *et al.* Non-infected preterm parturition is related to increased concentrations of IL-
670 6, IL-8 and MCP-1 in human cervix. *Reproductive Biology and Endocrinology* **3**, 1–10 (2005).
671 4. Frascoli, M. *et al.* Alloreactive fetal T cells promote uterine contractility in preterm labor via IFN-γ
672 and TNF-α. *Science Translational Medicine* **10**, (2018).
673 5. PrabhuDas, M. *et al.* Immune mechanisms at the maternal-fetal interface: Perspectives and
674 challenges. *Nature Immunology* **16**, 328–334 (2015).
675 6. Urbaniak, S. J. & Greiss, M. A. RhD haemolytic disease of the fetus and the newborn. *Blood*
676 *Reviews* **14**, 44–61 (2000).
677 7. Lee, J. *et al.* Maternal HLA Panel-Reactive Antibodies in Early Gestation Positively Correlate with
678 Chronic Chorioamnionitis: Evidence in Support of the Chronic Nature of Maternal Anti-fetal
679 Rejection. *American Journal of Reproductive Immunology* **66**, 510–526 (2011).
680 8. Bell, S. C. & Billington, W. D. Major anti-paternal alloantibody induced by murine pregnancy is
681 non-complement-fixing IgG1. *Nature* **288**, 387–388 (1980).
682 9. Suah, A. N. *et al.* Pregnancy-induced humoral sensitization overrides T cell tolerance to fetus-
683 matched allografts in mice. *Journal of Clinical Investigation* **131**, (2021).
684 10. Hönger, G. *et al.* Frequency and determinants of pregnancy-induced child-specific sensitization.
685 *American Journal of Transplantation* **13**, 746–753 (2013).
686 11. Küssel, L. *et al.* Longitudinal assessment of HLA and MIC-A antibodies in uneventful pregnancies
687 and pregnancies complicated by preeclampsia or gestational diabetes. *Scientific Reports* **7**, 1–10
688 (2017).

689 12. Thangaratinam, S. *et al.* Association between thyroid autoantibodies and miscarriage and preterm
690 birth: Meta-analysis of evidence. *Bmj* **342**, 1–8 (2011).
691 13. Wallukat, G. *et al.* Patients with preeclampsia develop agonistic autoantibodies against the
692 angiotensin AT1 receptor. *Journal of Clinical Investigation* **103**, 945–952 (1999).
693 14. Zhou, C. C. *et al.* Angiotensin receptor agonistic autoantibodies induce pre-eclampsia in pregnant
694 mice. *Nature Medicine* **14**, 855–862 (2008).
695 15. Yoshimura, K. & Hirsch, E. Effect of stimulation and antagonism of interleukin-1 signaling on
696 preterm delivery in mice. *J Soc Gynecol Investig* **12**, 533–538 (2005).
697 16. Romero, R. *et al.* A fetal systemic inflammatory response is followed by the spontaneous onset of
698 preterm parturition. *American Journal of Obstetrics and Gynecology* **179**, 186–193 (1998).
699 17. Romero, R., Mazor, M. & Tartakovsky, B. Systemic administration of interleukin-1 induces preterm
700 parturition in mice. *Am J Obstet Gynecol* **165**, 969–971 (1991).
701 18. Nadeau-Vallée, M. *et al.* Antenatal Suppression of IL-1 Protects against Inflammation-Induced
702 Fetal Injury and Improves Neonatal and Developmental Outcomes in Mice. *The Journal of*
703 *Immunology* **198**, 2047–2062 (2017).
704 19. Girard, S., Tremblay, L., Lepage, M. & Sébire, G. IL-1 Receptor Antagonist Protects against
705 Placental and Neurodevelopmental Defects Induced by Maternal Inflammation. *The Journal of*
706 *Immunology* **184**, 3997–4005 (2010).
707 20. Sadowsky, D. W., Adams, K. M., Gravett, M. G., Witkin, S. S. & Novy, M. J. Preterm labor is
708 induced by intraamniotic infusions of interleukin-1β and tumor necrosis factor-α but not by
709 interleukin-6 or interleukin-8 in a nonhuman primate model. *American Journal of Obstetrics and*
710 *Gynecology* **195**, 1578–1589 (2006).
711 21. Sadowsky, D. W., Haluska, G. J., Gravett, M. G., Witkin, S. S. & Novy, M. J. Indomethacin blocks
712 interleukin 1β–induced myometrial contractions in pregnant rhesus monkeys. *American Journal of*
713 *Obstetrics and Gynecology* **183**, 173–180 (2000).

714 22. Baggia, S., Gravett, M. G., Witkin, S. S., Haluska, G. J. & Novy, M. J. Interleukin-1 beta intra-
715 amniotic infusion induces tumor necrosis factor-alpha, prostaglandin production, and preterm
716 contractions in pregnant rhesus monkeys. *J Soc Gynecol Investig* **3**, 121–126 (1996).
717 23. Witkin, S. S., Gravett, M. G., Haluska, G. J. & Novy, M. J. Induction of interleukin-1 receptor
718 antagonist in rhesus monkeys after intraamniotic infection with group B streptococci or interleukin-
719 1 infusion. *Am J Obstet Gynecol* **171**, 1668–1672 (1994).
720 24. Gravett, M. G. *et al.* An experimental model for intraamniotic infection and preterm labor in rhesus
721 monkeys. *Am J Obstet Gynecol* **171**, 1660–1667 (1994).
722 25. Fidel Jr, P. I. *et al.* Interleukin-1 Receptor Antagonist (IL-1ra) Production by Human Amnion,
723 Chorion, and Decidua. *American Journal of Reproductive Immunology* **32**, 1–7 (1994).
724 26. Genc, M. R. *et al.* A disproportionate increase in IL-1β over IL-1ra in the cervicovaginal secretions
725 of pregnant women with alteredvaginal microflora correlates with preterm birth. *American Journal*
726 *of Obstetrics and Gynecology* **190**, 1191–1197 (2004).
727 27. Romero, R. *et al.* Interlukin-1 stimulates prostaglandin biosynthesis by human amnion.
728 *Prostaglandins* **37**, 13–22 (1989).
729 28. Heng, Y. J. *et al.* The interplay of the interleukin 1 system in pregnancy and labor. *Reproductive*
730 *Sciences* **21**, 122–130 (2014).
731 29. Yockey, L. J. & Iwasaki, A. Interferons and Proinflammatory Cytokines in Pregnancy and Fetal
732 Development. *Immunity* **49**, 397–412 (2018).
733 30. Stock, S. J. & Aiken, C. E. Barriers to progress in pregnancy research: How can we break
734 through? *Science* **380**, 150–153 (2023).
735 31. Chang, C. Y. *et al.* Withdrawing Approval of Makena — A Proposal from the FDA Center for Drug
736 Evaluation and Research. *New England Journal of Medicine* **383**, e131 (2020).
737 32. Busse, M. *et al.* Regulatory B Cells Are Decreased and Impaired in Their Function in Peripheral
738 Maternal Blood in Pre-term Birth. *Frontiers in Immunology* **11**, 1–10 (2020).

739 33. Rizzuto, G. *et al.* Establishment of fetomaternal tolerance through glycan-mediated B cell
740 suppression. *Nature* (2022) doi:10.1038/s41586-022-04471-0.
741 34. Yougbaré, I. *et al.* Maternal anti-platelet β3 integrins impair angiogenesis and cause intracranial
742 hemorrhage. *J Clin Invest* **125**, 1545–1556 (2015).
743 35. O'Donovan, B. *et al.* High-resolution epitope mapping of anti-Hu and anti-Yo autoimmunity by
744 programmable phage display. *Brain Communications* **2**, 1–16 (2020).
745 36. Larman, H. B. *et al.* Autoantigen discovery with a synthetic human peptidome. *Nature*
746 *Biotechnology* **29**, 535–541 (2011).
747 37. Larman, H. B. *et al.* PhIP-Seq characterization of autoantibodies from patients with multiple
748 sclerosis, type 1 diabetes and rheumatoid arthritis. *Journal of Autoimmunity* **43**, 1–9 (2013).
749 38. Porrett, P. M. Biologic mechanisms and clinical consequences of pregnancy alloimmunization.
750 *American Journal of Transplantation* **18**, 1059–1067 (2018).
751 39. Napso, T., Yong, H. E. J., Lopez-Tello, J. & Sferruzzi-Perri, A. N. The Role of Placental Hormones
752 in Mediating Maternal Adaptations to Support Pregnancy and Lactation. *Frontiers in Physiology* **9**,
753 (2018).
754 40. Vidal, M. S., Lintao, R. C. V., Severino, M. E. L., Tantengco, O. A. G. & Menon, R. Spontaneous
755 preterm birth: Involvement of multiple feto-maternal tissues and organ systems, differing
756 mechanisms, and pathways. *Frontiers in Endocrinology* **13**, (2022).
757 41. Ferrari, B. *et al.* Pregnancy complications in acquired thrombotic thrombocytopenic purpura: a
758 case–control study. *Orphanet J Rare Dis* **9**, 193 (2014).
759 42. Xiao, J. *et al.* Expression of ADAMTS13 in Normal and Abnormal Placentae and Its Potential Role
760 in Angiogenesis and Placenta Development. *Arteriosclerosis, Thrombosis, and Vascular Biology*
761 **37**, 1748–1756 (2017).
762 43. Sung, D. C. *et al.* VE-cadherin enables trophoblast endovascular invasion and spiral artery
763 remodeling during placental development. *eLife* **11**, e77241.

764 44. Leach, L. The phenotype of the human materno-fetal endothelial barrier: molecular occupancy of
765 paracellular junctions dictate permeability and angiogenic plasticity. *J Anat* **200**, 599–606 (2002).
766 45. Lee, J. *et al.* Detection of anti-HLA antibodies in maternal blood in the second trimester to identify
767 patients at risk for antibody-mediated maternal anti-fetal rejection and spontaneous preterm
768 delivery. *Am J Reprod Immunol* **70**, 162–175 (2013).
769 46. Bastard, P. *et al.* Autoantibodies against type I IFNs in patients with life-threatening COVID-19.
770 *Science* **370**, (2020).
771 47. Schreuder, H. *et al.* A new cytokine-receptor binding mode revealed by the crystal structure of the
772 IL-1 receptor with an antagonist. *Nature* **386**, 194–200 (1997).
773 48. Krishnan, S. & Raibekas, A. A. Multistep Aggregation Pathway of Human Interleukin-1 Receptor
774 Antagonist : Kinetic , Structural , and Morphological Characterization. *Biophysj* **96**, 199–208
775 (2009).
776 49. Jarrell, J. A. *et al.* Neutralizing anti-IL-1 receptor antagonist autoantibodies induce inflammatory
777 and fibrotic mediators in IgG4-related disease. *J Allergy Clin Immunol* **149**, 358–368 (2022).
778 50. Thurner, L. *et al.* IL-1RA Antibodies in Myocarditis after SARS-CoV-2 Vaccination. *N Engl J Med*
779 **387**, 1524–1527 (2022).
780 51. Pfeifer, J. *et al.* Autoantibodies against interleukin-1 receptor antagonist in multisystem
781 inflammatory syndrome in children: a multicentre, retrospective, cohort study. *The Lancet*
782 *Rheumatology* **4**, e329–e337 (2022).
783 52. Wing, D. A. *et al.* Placental Alpha Microglobulin-1 Compared With Fetal Fibronectin to Predict
784 Preterm Delivery in Symptomatic Women. *Obstet Gynecol* **130**, 1183–1191 (2017).
785 53. Practice Bulletin No. 159: Management of Preterm Labor. *Obstetrics & Gynecology* **127**, e29
786 (2016).
787 54. American College of Obstetricians and Gynecologists (ACOG). Practice Bulletin 713. Antenatal
788 Corticosteroid Therapy for Fetal Maturation. *Obstetrics and gynecology* **133**, 404–405 (2017).

789 55. Ikonomidis, I. *et al.* Inhibition of Interleukin-1 by Anakinra Improves Vascular and Left Ventricular
790 Function in Patients With Rheumatoid Arthritis. *Circulation* **117**, 2662–2669 (2008).
791 56. Hoffmann, M.-C. *et al.* Autoantibody-Mediated Depletion of IL-1RA in Still's Disease and Potential
792 Impact of IL-1 Targeting Therapies. *J Clin Immunol* **44**, 45 (2024).
793 57. Murtha, A. P. *et al.* Association of maternal IL-1 receptor antagonist intron 2 gene polymorphism
794 and preterm birth. *American Journal of Obstetrics and Gynecology* **195**, 1249–1253 (2006).
795 58. Vazquez, S. E. *et al.* Autoantibody discovery across monogenic, acquired, and COVID-19-
796 associated autoimmunity with scalable PhIP-seq. *eLife* **11**, e78550 (2022).
797 59. Zhang, L., McAlpine, P. L., Heberling, M. L. & Elias, J. E. Automated Ligand Purification Platform
798 Accelerates Immunopeptidome Analysis by Mass Spectrometry. *J. Proteome Res.* **20**, 393–408
799 (2021).
800 60. Meier, F. *et al.* diaPASEF: parallel accumulation–serial fragmentation combined with data-
801 independent acquisition. *Nat Methods* **17**, 1229–1236 (2020).
802 61. 'Signal Processing Methods for Power Doppler Microvascular Angiography' by Mai H.
803 Elfarnawany. https://ir.lib.uwo.ca/etd/3106/.
804 62. Zhao, Y., Tang, H. & Ye, Y. RAPSearch2: a fast and memory-efficient protein similarity search
805 tool for next-generation sequencing data. *Bioinformatics* **28**, 125–126 (2012).
806 63. Vazquez, S. E. *et al.* Identification of novel, clinically correlated autoantigens in the monogenic
807 autoimmune syndrome APS1 by proteome-wide PhIP-Seq. *eLife* **9**, 1–25 (2020).
808 64. Rajan, J. V. *et al.* Phage display demonstrates durable differences in serological profile by route of
809 inoculation in primary infections of non-human primates with Dengue Virus 1. *Scientific Reports*
810 **11**, 1–12 (2021).
811
812
813
814
815
816
817
818

ACKNOWLEDGEMENTS

We thank members of the DeRisi Lab for helpful discussions and JM Rackaitis for support during these studies. We thank Joelle Ostroff for inspiring the studies herein. We also acknowledge the New York Blood Center for contribution of healthy control plasma. We thank the UCSF CALM-NIC microscopy core for use of the CREST LFOV Spinning Disk/C2 confocal funded by the UCSF Program for Breakthrough Biomedical Research, the Sandler Foundation, Strategic Advisory Committee, and the EVCP Office Research Resource Program Institutional Matching Instrumentation Award. ER is funded by 2022 Next Gen Pregnancy Initiative Research Grant from the Burroughs Wellcome Fund, the Eunice Kennedy Shriver National Institute of Child Health and Human Development award 5T32HD098057, and National Institute of Allergy and Infectious Diseases award K99AI182451. CMB is funded by The Emiko Terasaki Foundation (project 7027742/fund B73335) and by the National Institute of Neurological Disorders and Stroke of the NIH award K99NS117800. GR is funded by National Institute of Allergy and Infectious Diseases award K08AI137209. SLG is supported by National Institute of Allergy and Infectious Diseases award K08AI141728. JLD is funded by a grant from Chan Zuckerberg Biohub. Contents herein are the sole responsibility of the authors and do not necessarily represent the official views of the NIH or other funding agencies.

AUTHOR CONTRIBUTIONS

ER and JLD designed the research. ER, BB, SJS, JSC, HMK, EK, MM, SAM, FM, SO, KCZ, AM, GR, RJB performed the research. ER, HMK, HSM, AFK, CMB, JSC, FM, JEE, and JLD contributed to new reagents and analytic tools. SJS, SLG, KKR, LLJP, JH, and NCS provided clinical samples, metadata, and/or contributed to clinical interpretation of data. JSC, FM, and JEE generated and analyzed mass spectrometry datasets. BB and TCM provided significant contributions to mouse model development. ER and JLD analyzed data and produced figures. ER and JLD wrote the manuscript. All authors reviewed the manuscript and provided feedback.

COMPETING INTERESTS

ER and JLD are inventors on a patent application submitted by the Regents of the University of California and the Chan Zuckerberg Biohub San Francisco that covers serological prediction of preterm delivery and the use of IL1RA for therapeutic prevention of preterm labor.

MATERIALS AND CORRESPONDENCE

Correspondence and requests for materials should be addressed to Joseph L. DeRisi, joe@derisilab.ucsf.edu.

Figure 1

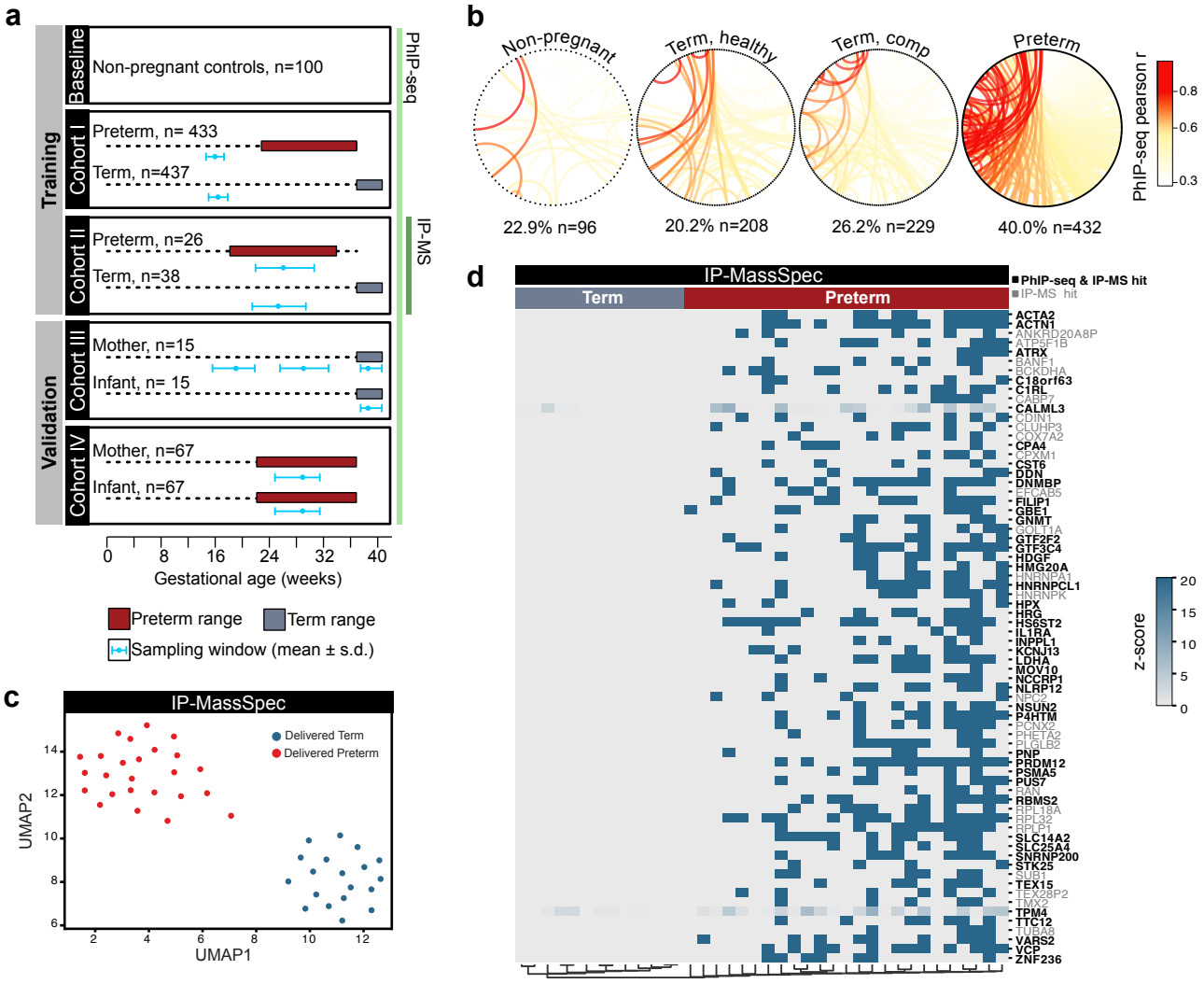

Figure 1. Maternal autoantibody signature is predictive of spontaneous preterm delivery by PhIP-seq and IP-MS **a.** Schematic of study design integrating data from four cohorts of human pregnancy subjected to human peptidome PhIP-seq and/or IP-MS with placental lysate and one baseline cohort of non-pregnant controls. Sampling range indicated in cyan, delivery timepoints indicated in dark red or dark blue for preterm or term pregnancies, respectively. Data from training cohorts was kept separate from validation cohorts to prevent data leakage. **b**. Co-correlation analysis of PhIP-seq signatures between healthy non-pregnant, term and preterm pregnancies. Pearson correlation coefficients greater than 0.3 are colored to scale bar, percent connectivity indicates proportion of connected nodes. Each node represents serum from one person. **c.** Unsupervised UMAP analysis of placental IP-MS protein abundances in Cohort II, colored by subsequent term (blue) or preterm (red) delivery. **d.** Heatmap of hierarchically clustered z-scores from top 70 preterm-specific reactivities by placental IP-mass spec. Bolded protein names indicate that the hit was also identified by PhIP-seq, while gray prein names indicate the hit was identified by IP-MS only.

Figure 2

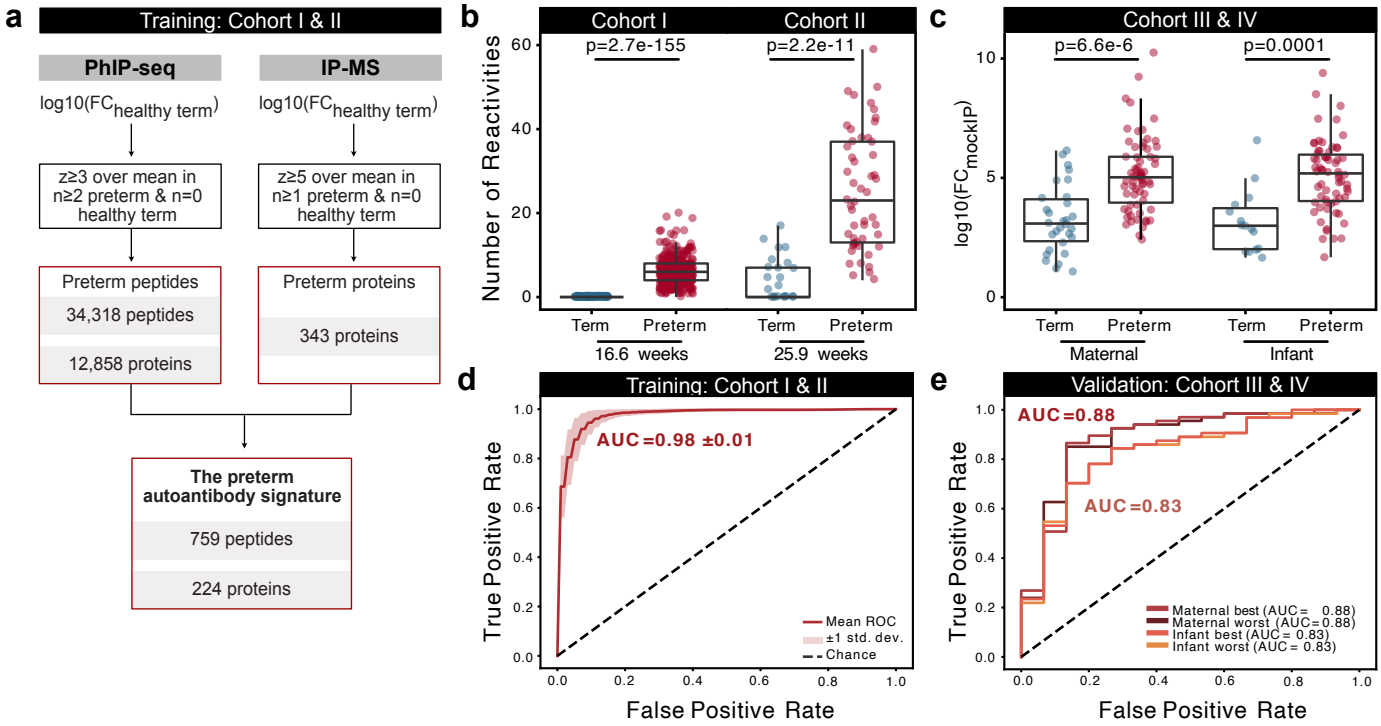

Figure 2. ***Autoantibody screening test for preterm delivery in validation cohorts***
a. Flow chart of feature selection to identify the preterm autoantibody signature. Z-scored log10 fold change (FC) over healthy term pregnancies was used to filter hits by prevalence from PhIP-seq data (Cohort I) and IP-MS data (Cohort II). The overlap of proteins identified by both techniques was selected as the preterm autoantibody signature and used for downstream analysis. **b.** Number of PhIP-seq and IP-MS validated preterm-specific autoantibody reactivities in term (blue) and preterm (red) pregnancies in Cohort I (left) and Cohort II (right). **c.** Sum log10 fold-change of over mock-IP of preterm-specific autoreactivities identified in maternal (left) or infant (right) samples in Cohorts III-IV. Receiver operator curve analysis of a forecasting model built on the autoantibody signature from Cohorts I & II and tested on the **d.** training cohorts (Cohorts I and II) across 1000 shuffles of stratified five-fold cross-validation iterations and **e.** performance of the best and worst model from training in test cohorts (Cohorts III and IV). PhIP-seq data filtered for conserved features across PhIP-seq and IP-MS datasets was used to generate models and graphs. Kolmogorov-Smirnov pairwise test for significance in b-c.

Figure 3

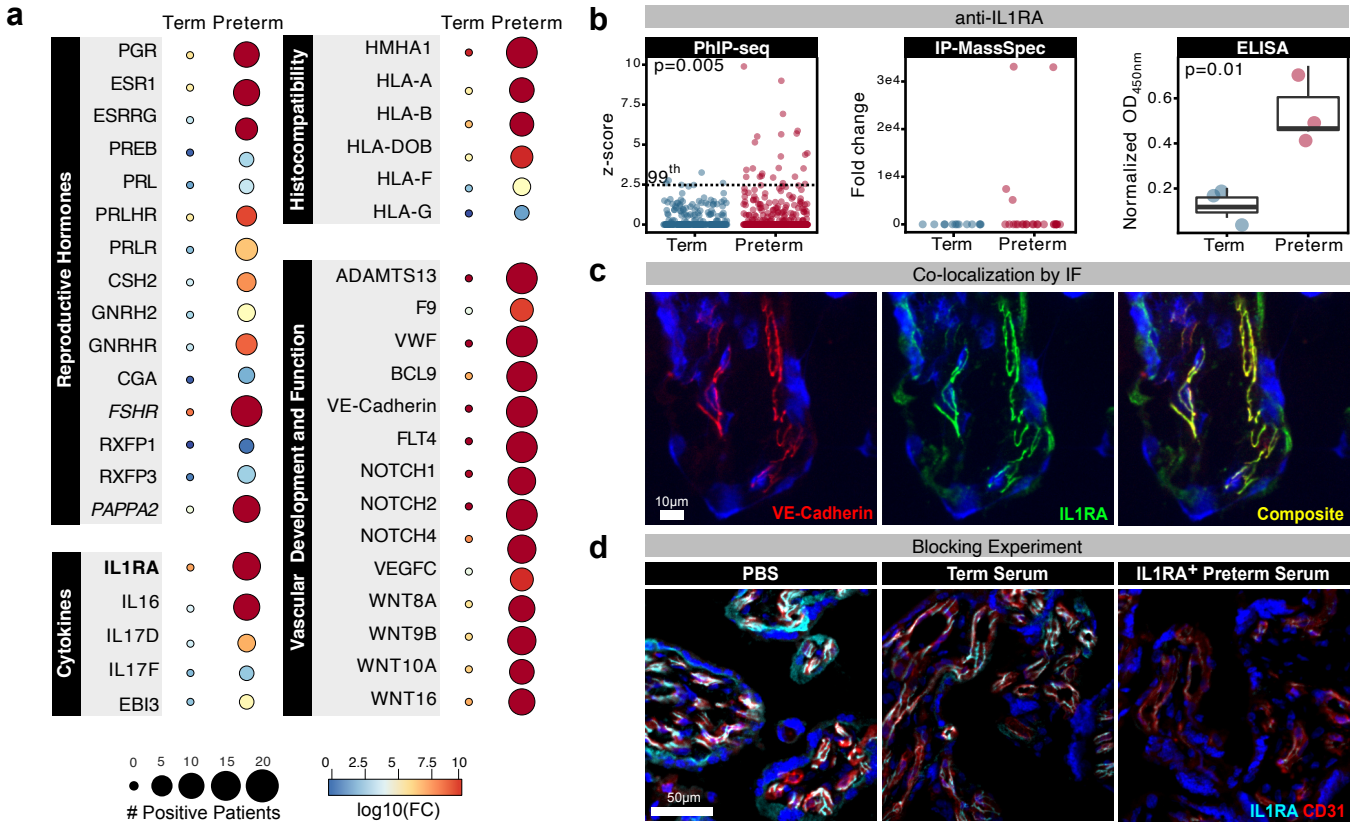

Figure 3. Autoantibody signature specific to subsequent preterm delivery
a. Dot plot of selected autoreactive targets in term (left) and preterm (right) pregnancies in Cohort I within selected pathways. Dots are scaled to the number of positive patients and colored by log10 fold change above mean term pregnancy. **b**. anti-IL1RA antibodies in preterm versus term pregnancies as detected by z-score of fold change above mean in term pregnancies detected by PhIP-seq in Cohort I (left), fold change over mean in term pregnancies detected by placental IP-MS in Cohort II (middle), or normalized optical density (OD_{450}) relative to assay blanks in ELISA utilizing HEK293T IL1RA overexpression lysate as bait for selected patient sera from Cohort II (left). Spinning disk confocal micrographs of indirect immunofluorescence of placenta probed with **c**. anti-VE-cadherin (left) or anti-IL1RA antibody (middle). Composite (right) indicates overlay of signal from anti-VE-cadherin and anti-IL1RA. **d.** Spinning disk confocal micrographs of indirect immunofluorescence of placenta preblocked with PBS, term sera, or anti-IL1RA^{+} preterm sera from Cohort II. Overlay of signal from anti-CD31 (red), anti-IL1RA (cyan), and DAPI (blue). DAPI counterstain in blue; scale bar corresponds to 10µm in c and 50µm in d. Dotted line indicates 99th percentile in term pregnancies used to calculate odds ratio p-value in b. Kolmogorov-Smirnov pairwise test for significance in b.

Figure 4

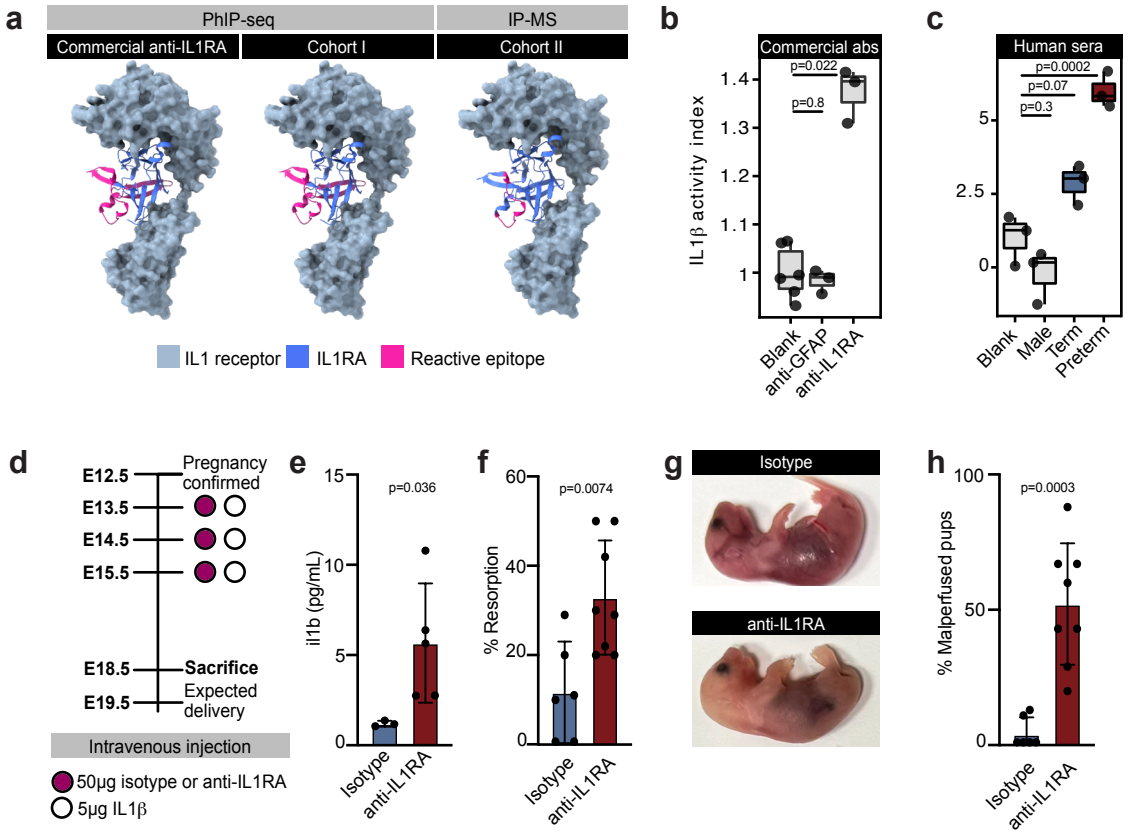

Figure 4. Anti-IL1RA antibodies in preterm sera functionally inhibit IL antagonism
a. Location of reactive epitope (magenta) determined by PhIP-seq or IP-MS for an anti-IL1RA commercial antibody or enriched in preterm sera in Cohort I or Cohort II on the structure of human IL1RA (green) bound to the IL1 receptor (blue). PDB accession: 1IRA. Quantification of secreted embryonic alkaline phosphatase (SEAP) produced by HEK-Blue IL-1β reporter cells incubated with human IL-1β and IL-1RA in the presence of **b.** PBS, off target anti-GFAP, or anti-IL1RA polyclonal antibody or **c.** male, term, anti-IL1RA^{+} sera or no serum controls. IL1 activity was calculated by dividing experimental signal with patient sera by cells treated with IL1 alone. **d.** Schematic of injections in timed-pregnant C57Bl/6 mice. Isotype or anti-IL1RA commercial antibody was injected daily on embryonic days (E) 13.5-15.5; mice were sacrificed on E18.5. Quantification of **e.** Il1b (pg/mL) in maternal serum by ELISA, **f.** complete resorption rate (%), **g**. representative images of non-resorbed pups, **h**. percentage of malperfused pups among live pups in isotype or anti-IL1RA injected dams at E18.5. Statistical significance calculated by one-way ANOVA with Tukey post-hoc in b-c or Kolmogorov-Smirnov pairwise test in e,f,h.

Extended Data Figure 1

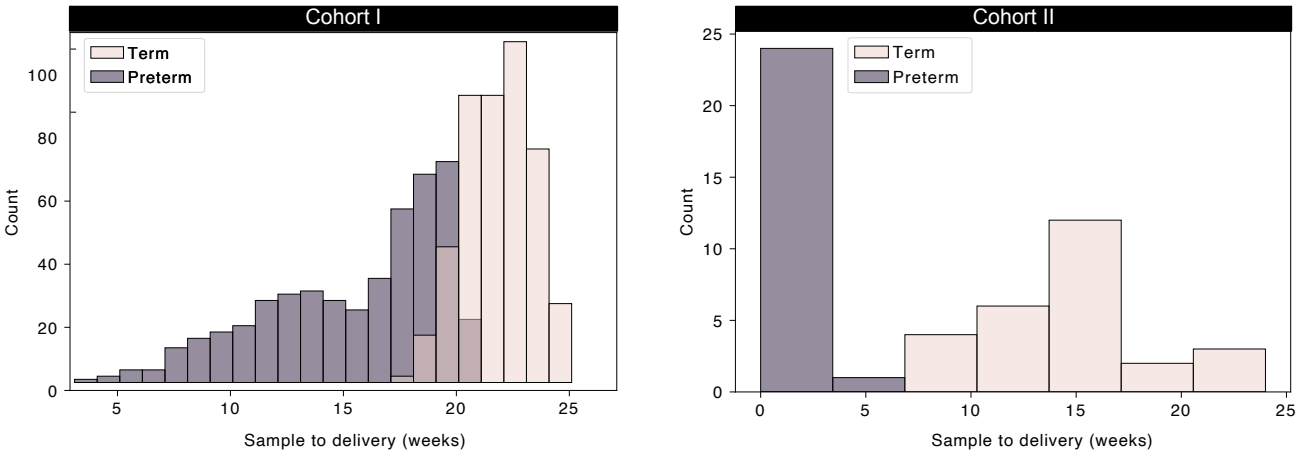

Extended Data Figure 1. **Maternal serum sample time relative to delivery time in Cohorts I and II.** Histograms of sample time to delivery in weeks in preterm (purple) or term (yellow) pregnancies within **a.** Cohort I and **b.** Cohort II

Extended Data Figure 2

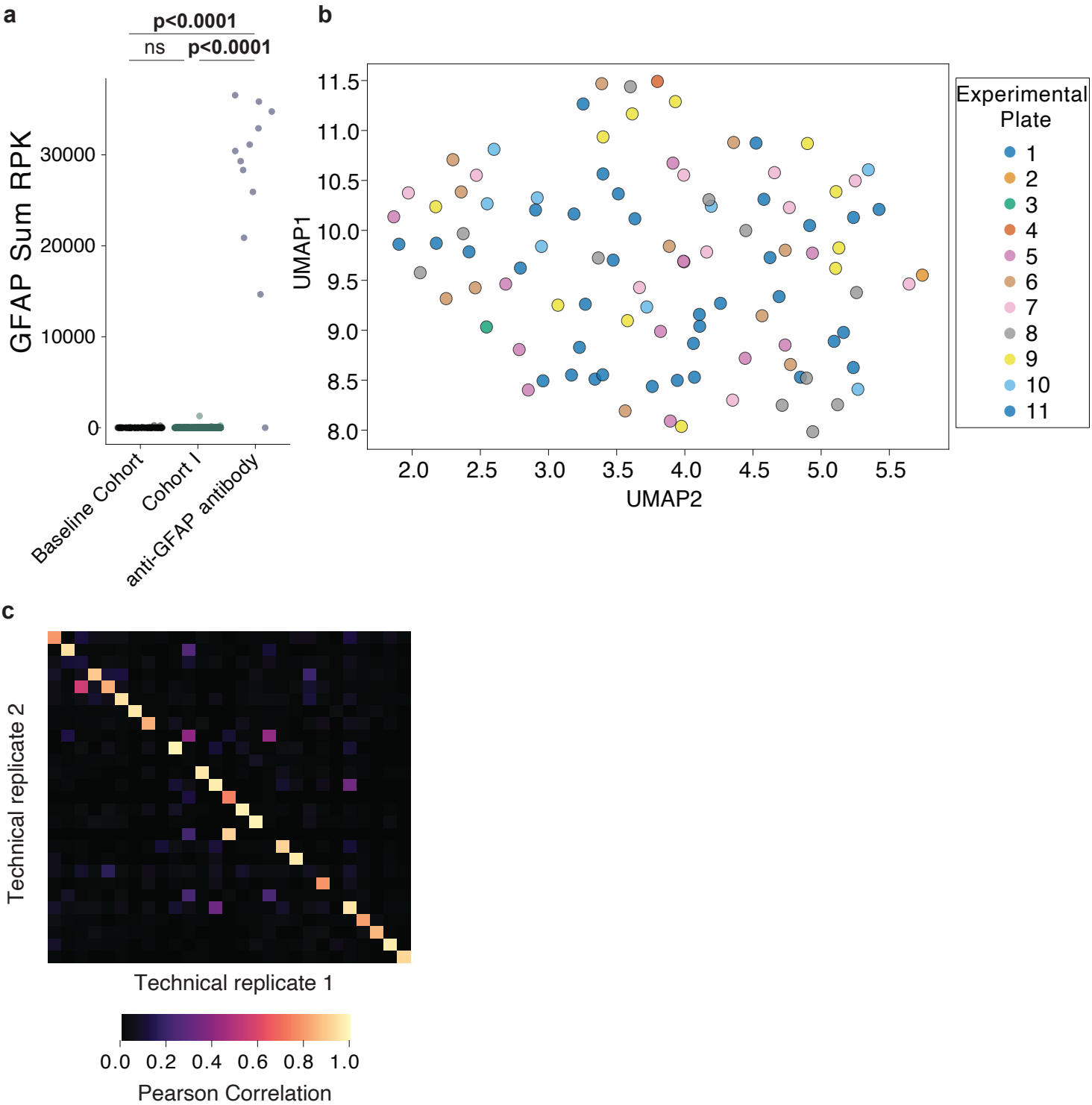

Extended Data Figure 2. **Technical consistency of the PhIP-seq method. a.** Sum reads per 100,000 (RPK) of peptides within GFAP protein in immunoprecipitations (IPs) with sera from the Baseline cohort or Cohort I, and with anti-GFAP antibody. **b**. UMAP analysis of baseline serum IP enrichments across experimental plates (batches). **c.** Pearson co-correlation analysis of technically replicated samples from baseline cohort. Enrichments identified by PhIP-seq in a-c.

Extended Data Figure 3

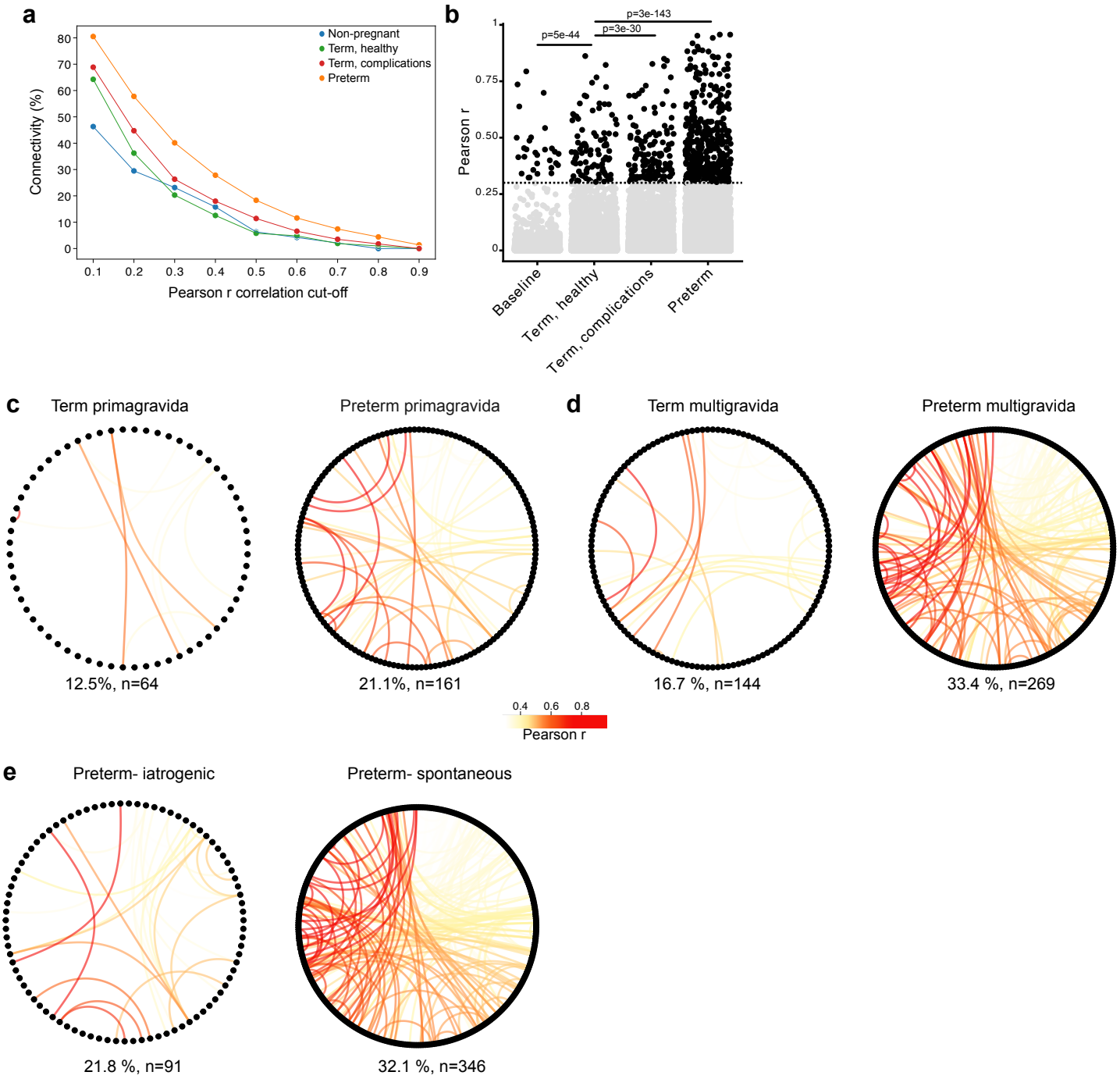

Extended Data Figure 3. Effect of gravidity and preterm phenotypes in PhIP-seq signatures. a. Percent connectivity relative to Pearson r co-correlation cut-off or **b.** Pearson r in non-pregnant, uncomplicated and complicated term, or preterm pregnancies. Co-correlation analysis of PhIP-seq signatures between **c**. term and preterm primigravida, **d.** term and preterm multigravida, or **e.** iatrogenic or spontaneous preterm pregnancies from Cohort I. Pearson correlation coefficients greater than 0.3 are colored to scale bar, mean degree of connectivity indicates proportion of connected nodes. Each node represents serum from one person. Kruskal-Wallis test for significance with Dunn's post-hoc in b.

Extended Data Figure 4

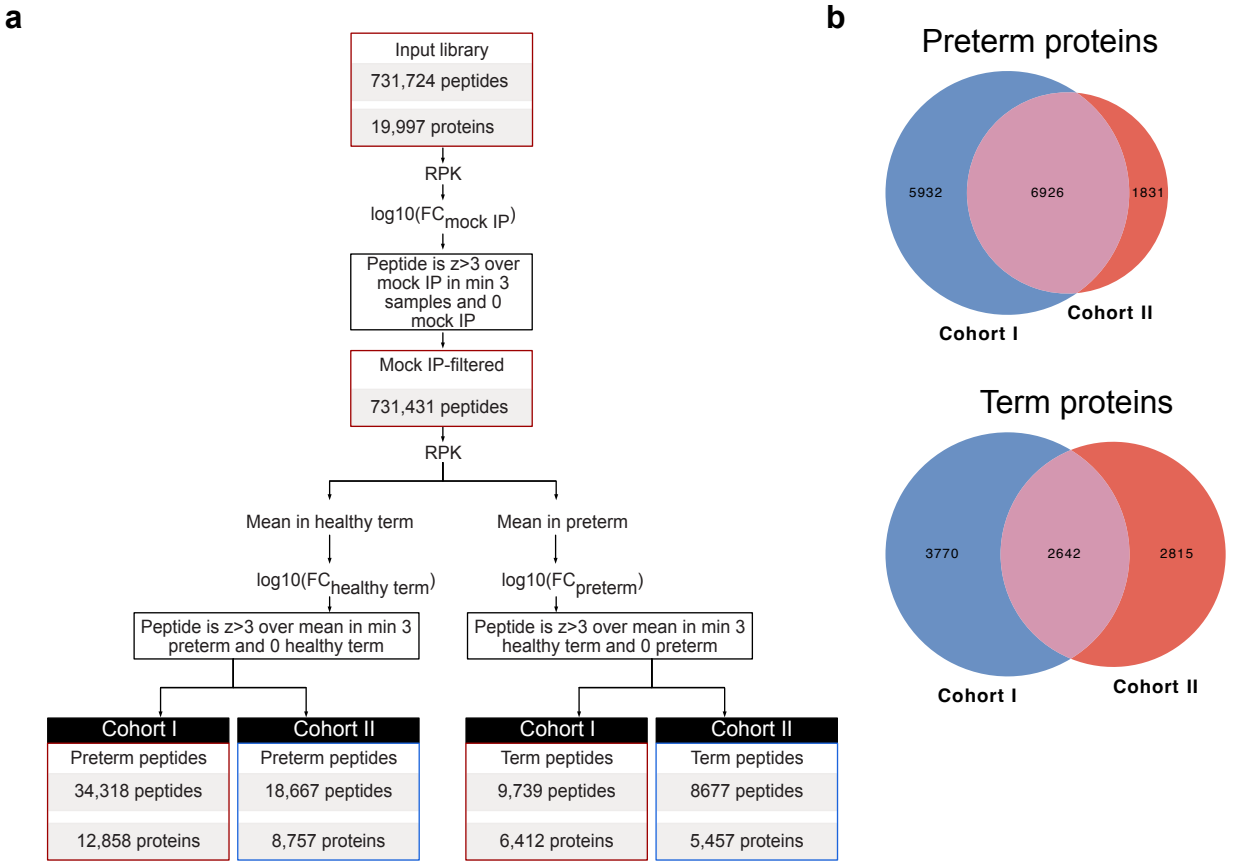

Extended Data Figure 4. Identification of term- and preterm-specific autoreactivities by PhIP-seq. **a.** Flow chart of hit filtering strategy from input peptide library to term and preterm specific hits for Cohort I and Cohort II. **b.** Overlap of preterm (top) and term (bottom) specific reactivities at the protein level between Cohort I and Cohort II.

Extended Data Figure 5

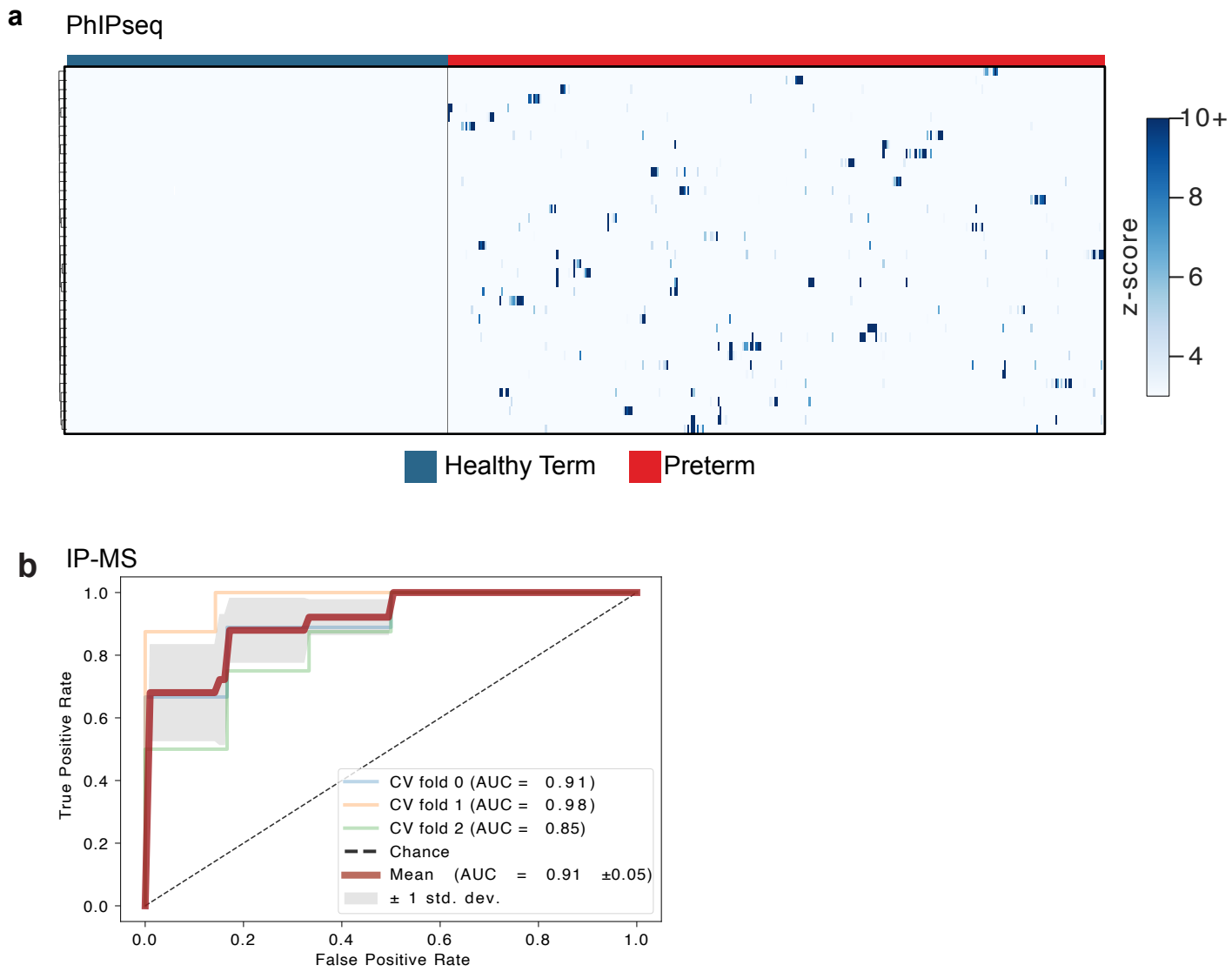

Extended Data Figure 5. Feature selection and initial logistic regression classifier to predict preterm delivery from PhIP-seq and IP-MS datasets. a. Heatmap of z-scores above non-pregnant baselines of top 50 autoantibody reactivities identified by PhIP-seq in healthy term or preterm pregnancies in Cohort I. **b.** Receiver operating characteristic curve (ROC) of the performance of a ridge-regularized logistic regression classifier trained on placental IP-MS data from the Cohort II and tested in 3-fold cross validation.

Extended Data Figure 6

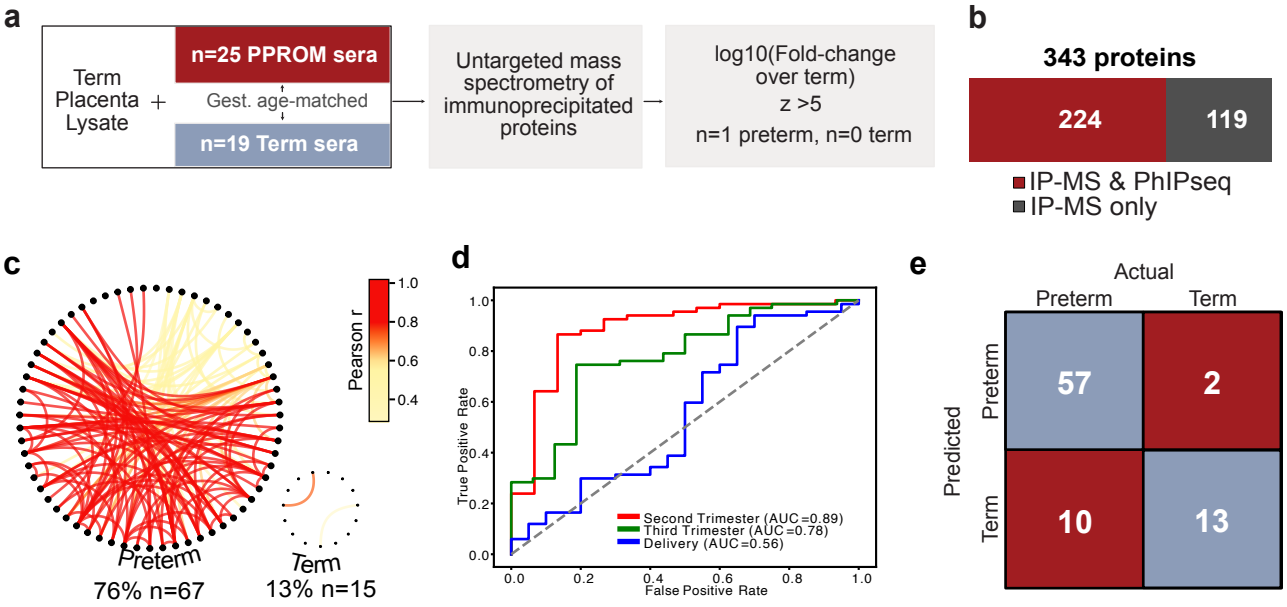

Extended Data Figure 6. Validation and performance evaluation of preterm-specific autoantibody signature. a. Schematic of the placental IP-MS experiment and hit filtration approach (left) **b.** Barplot of preterm-specific autoreactivities in IP-MS analysis that overlap with those identified by PhIP-seq. **c.** Inter-dyad co-correlation coefficients of preterm-specific PhIP-seq signatures within maternal sera from term (Cohort III) or preterm (Cohort IV) pregnancies. Pearson correlation coefficients greater than 0.3 are colored to scale bar, mean degree of connectivity indicates proportion of connected nodes. Each node represents serum from one person. **d.** Receiver operating characteristic curve (ROC) of the performance of the final ensemble model to predict preterm pregnancy, when provided with term samples from the second or third trimerster or delivery timepoints. **e.** Confusion matrix of the final ensemble model with a true positive rate cut-off of 0.8 in Cohorts III and IV.

Extended Data Figure 7

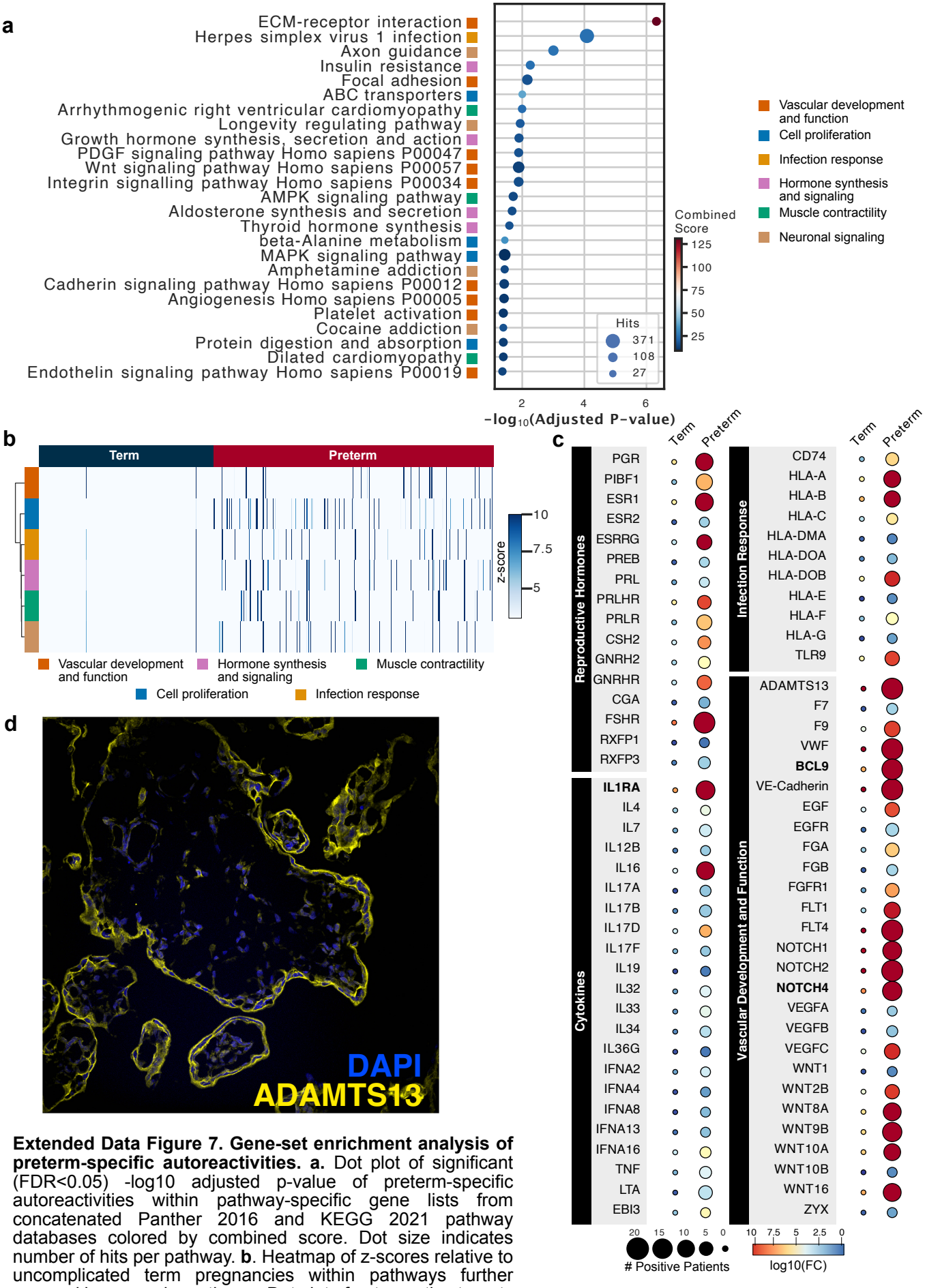

Extended Data Figure 7. Gene-set enrichment analysis of preterm-specific autoreactivities. a. Dot plot of significant (FDR<0.05) -log10 adjusted p-value of preterm-specific autoreactivities within pathway-specific gene lists from concatenated Panther 2016 and KEGG 2021 pathway databases colored by combined score. Dot size indicates number of hits per pathway. **b**. Heatmap of z-scores relative to uncomplicated term pregnancies within pathways further grouped by manual curation. **c.** Dot plot of autoreactive targets in term (left) and preterm (right) pregnancies in Cohort I within selected pathways. Dots are scaled to the number of positive patients and colored by log10 fold change above mean term pregnancy. **d.** Immunofluorescence of placenta probed with anti-ADAMTS13 (yellow) and counterstained with DAPI.

Extended Data Figure 8

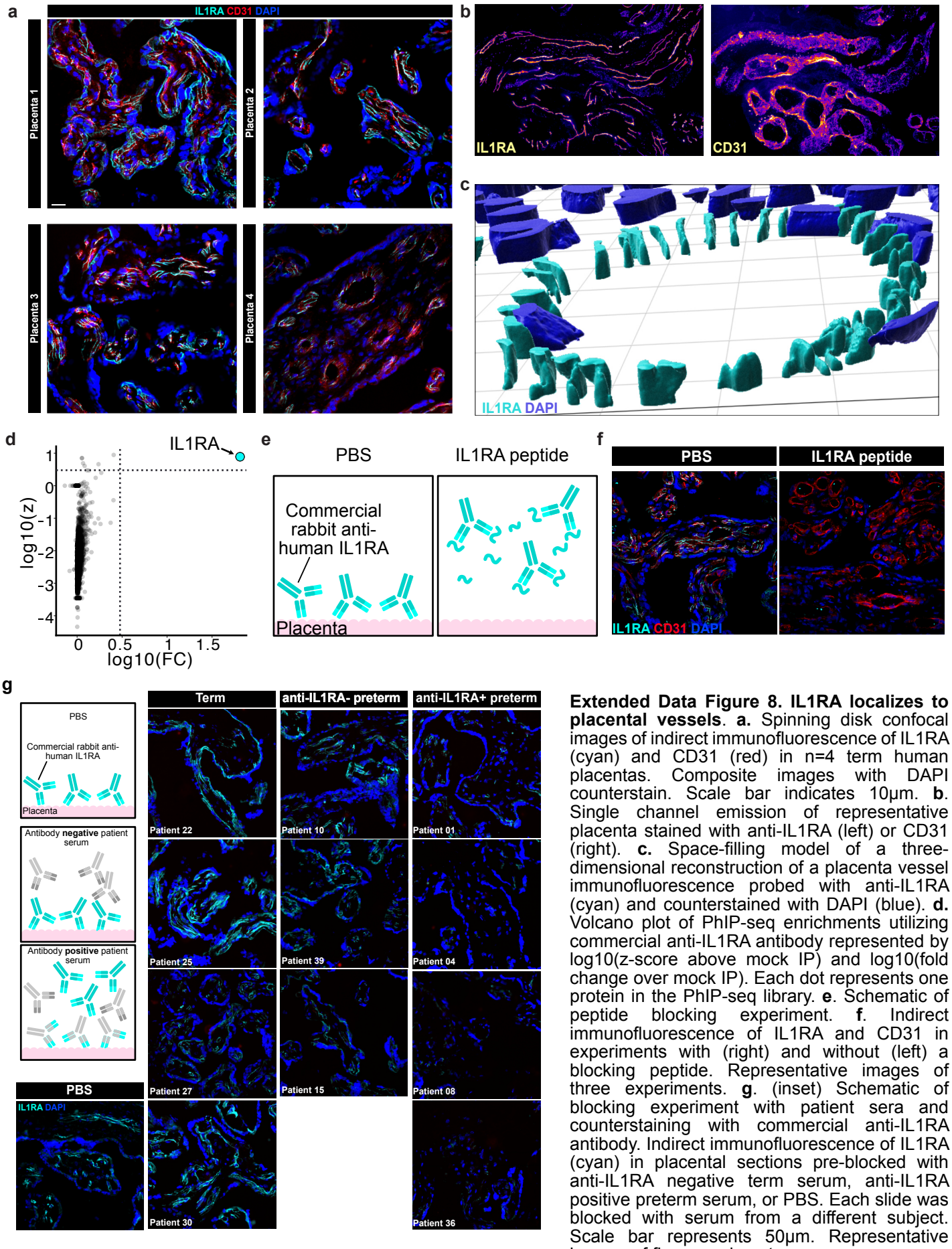

Extended Data Figure 8. IL1RA localizes to placental vessels. **a.** Spinning disk confocal images of indirect immunofluorescence of IL1RA (cyan) and CD31 (red) in n=4 term human placentas. Composite images with DAPI counterstain. Scale bar indicates 10µm. **b**. Single channel emission of representative placenta stained with anti-IL1RA (left) or CD31 (right). **c.** Space-filling model of a three-dimensional reconstruction of a placenta vessel immunofluorescence probed with anti-IL1RA (cyan) and counterstained with DAPI (blue). **d.** Volcano plot of PhIP-seq enrichments utilizing commercial anti-IL1RA antibody represented by log10(z-score above mock IP) and log10(fold change over mock IP). Each dot represents one protein in the PhIP-seq library. **e**. Schematic of peptide blocking experiment. **f**. Indirect immunofluorescence of IL1RA and CD31 in experiments with (right) and without (left) a blocking peptide. Representative images of three experiments. **g**. (inset) Schematic of blocking experiment with patient sera and counterstaining with commercial anti-IL1RA antibody. Indirect immunofluorescence of IL1RA (cyan) in placental sections pre-blocked with anti-IL1RA negative term serum, anti-IL1RA positive preterm serum, or PBS. Each slide was blocked with serum from a different subject. Scale bar represents 50µm. Representative images of five experiments.

Extended Data Figure 9

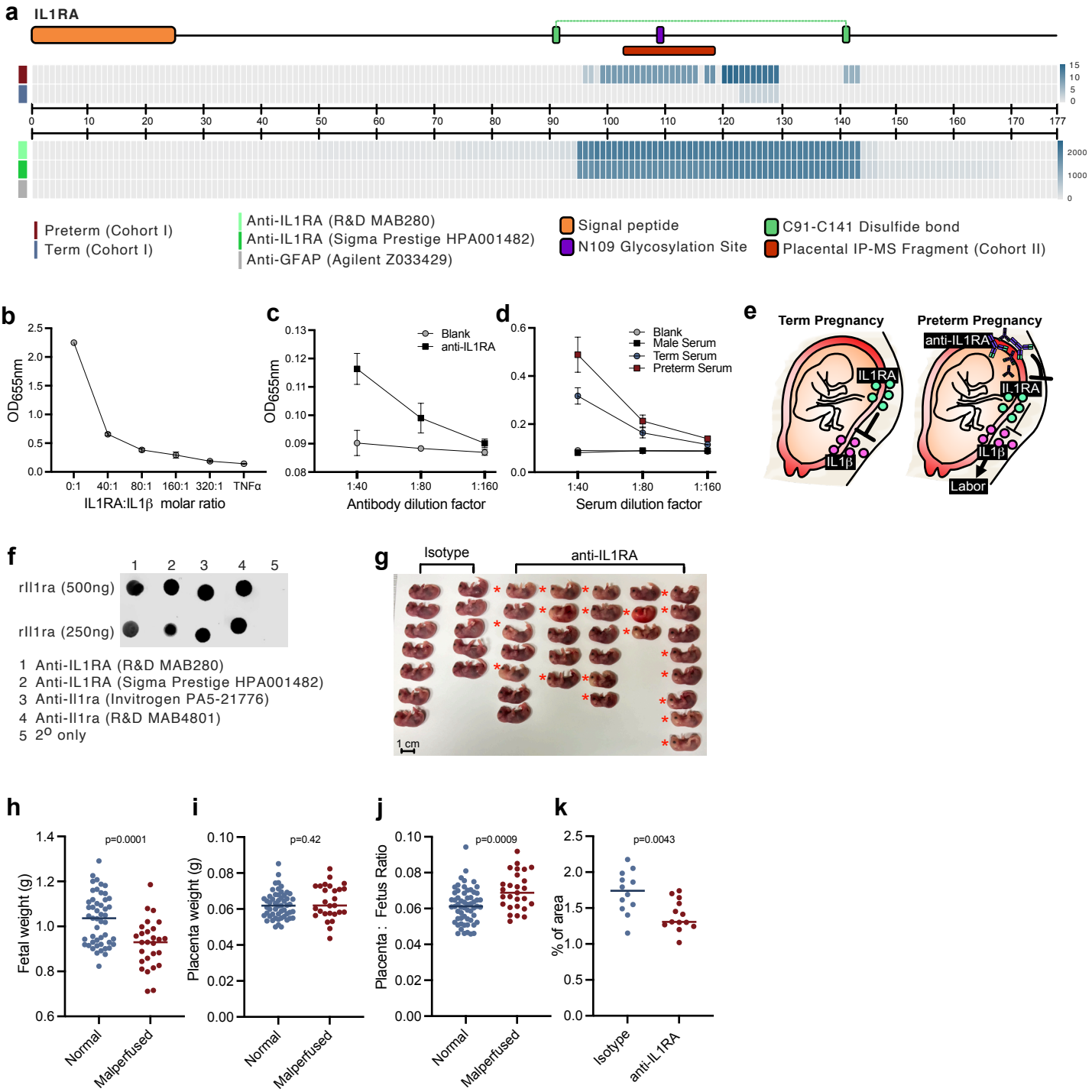

Extended Data Figure 9. Neutralizing anti-IL1RA antibodies dysregulate IL1. **a.** Domain structure of IL1RA with placental IP-MS fragment enriched in preterm pregnancies in Cohort II (red; top). Heatmap of mean corresponding positional enrichment for each amino acid by PhIP-seq in term and preterm pregnancies in Cohort I (middle) or in IPs with commercial anti-IL1RA or off-target anti-GFAP antibodies. SEAP activity in HEKBlue IL1 reporter cell line as measured by the conversion of a chromogenic substrate at OD_{655} in titration experiments of **b.** decreasing IL1RA **c**. anti-IL1RA antibody, or **d.** sera from a male donor or term or preterm pregnancy. **e.** Dot blot of recombinant mouse 500ng (top) or 250ng (bottom) Il1ra probed with anti-human IL1RA antibodies (lanes 1-2), or anti-mouse Il1ra (lanes 3-4), or secondary only control (lane 5). **f.** Representative images of fetuses from isotype or anti-IL1RA injected mice. Each column represents pups from one dam, asterisk indicated observation of gross vascular defects. **g.** Fetal weight (g), **h.** placental weight (g), **i.** or the placental: fetus weight ratio for fetuses classified as normal or malperfused. **j.** Image quantification of cephalic vasculature of non-resorbed pups in isotype or anti-IL1RA treated mice. KS test for significance in g-j.